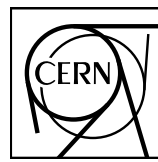


EUROPEAN ORGANIZATION FOR NUCLEAR RESEARCH



CERN-EP-2022-061

24 March 2022

Elliptic flow of charged particles at midrapidity relative to the spectator plane in Pb–Pb and Xe–Xe collisions

ALICE Collaboration*

Abstract

Measurements of the elliptic flow coefficient relative to the collision plane defined by the spectator neutrons $v_2 \{\Psi_{\text{SP}}\}$ in collisions of Pb ions at center-of-mass energy per nucleon–nucleon pair $\sqrt{s_{\text{NN}}} = 2.76 \text{ TeV}$ and Xe ions at $\sqrt{s_{\text{NN}}} = 5.44 \text{ TeV}$ are reported. The results are presented for charged particles produced at midrapidity as a function of centrality and transverse momentum for the 5–70% and 0.2–6 GeV/c ranges, respectively. The ratio between $v_2 \{\Psi_{\text{SP}}\}$ and the elliptic flow coefficient relative to the participant plane $v_2 \{4\}$, estimated using four-particle correlations, deviates by up to 20% from unity depending on centrality. This observation differs strongly from the magnitude of the corresponding eccentricity ratios predicted by the T_RENTo and the elliptic power models of initial state fluctuations that are tuned to describe the participant plane anisotropies. The differences can be interpreted as a decorrelation of the neutron spectator plane and the reaction plane because of fragmentation of the remnants from the colliding nuclei, which points to an incompleteness of current models describing the initial state fluctuations. A significant transverse momentum dependence of the ratio $v_2 \{\Psi_{\text{SP}}\} / v_2 \{4\}$ is observed in all but the most central collisions, which may help to understand whether momentum anisotropies at low and intermediate transverse momentum have a common origin in initial state fluctuations. The ratios of $v_2 \{\Psi_{\text{SP}}\}$ and $v_2 \{4\}$ to the corresponding initial state eccentricities for Xe–Xe and Pb–Pb collisions at similar initial entropy density show a difference of $(7.0 \pm 0.9)\%$ with an additional variation of $+1.8\%$ when including RHIC data in the T_RENTo parameter extraction. These observations provide new experimental constraints for viscous effects in the hydrodynamic modeling of the expanding quark–gluon plasma produced in heavy-ion collisions at the LHC.

© 2022 CERN for the benefit of the ALICE Collaboration.

Reproduction of this article or parts of it is allowed as specified in the CC-BY-4.0 license.

*See Appendix A for the list of collaboration members

Determining the properties of deconfined quark–gluon matter, called quark–gluon plasma (QGP), is the goal of the heavy-ion program at the Large Hadron Collider (LHC). Previous studies of data collected at the Brookhaven Relativistic Heavy-Ion Collider (RHIC) and the LHC have shown that the QGP behaves like a liquid with very small specific shear and bulk viscosities [1, 2]. In heavy-ion collisions, these properties are encoded in the collective expansion of the strongly interacting QGP. Measurements of this collective behavior, in particular the anisotropic flow driven by the spatial anisotropy of the shape of the overlap region of the colliding nuclei, can be used to infer the QGP transport properties. The anisotropic flow is quantified by the coefficients v_n of a Fourier decomposition of the momentum anisotropy of emitted particles relative to the collision symmetry planes with angles Ψ_n of the harmonic n . The dominant coefficient in off-center collision of heavy ions is the elliptic flow v_2 . The shape of the initial energy density distribution in the overlap region of the nuclei (participant zone) fluctuates from collision to collision due to the motion of nucleons and the quantum mechanical nature of the nucleus–nucleus interaction, which is typically modeled by spatial position fluctuations of the interacting nucleons. This was initially discussed in the context of the elliptic flow fluctuations [3–5] and later confirmed by observations [6–10] of significant non-zero triangular flow v_3 and higher flow harmonics. A detailed picture of fluctuations has already been inferred from the comparison of initial state models to measurements of flow fluctuations relative to the participant symmetry planes [8, 11–28]. Additional information about the pattern of initial state fluctuations can be obtained from measurements using spectator nucleons, which decouple very fast from the participant zone.

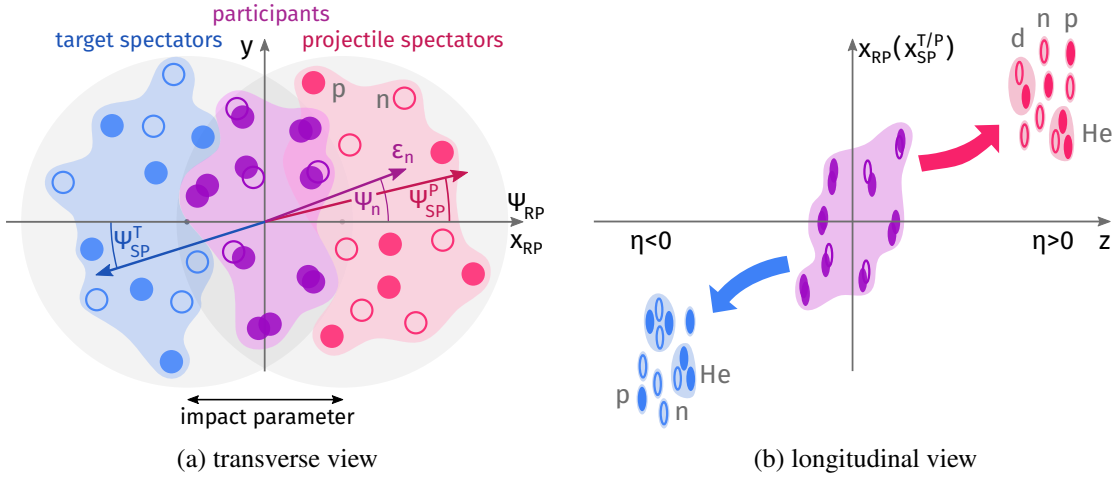


Figure 1: (color online) A sketch of the geometry of a non-central heavy-ion collision in the (a) transverse (x_{RP}, y) and (b) reaction (x_{RP}, z) planes. The x_{RP} axis points along the direction of the impact parameter given by the distance between the centers of the colliding nuclei, while the z axis is oriented along the direction of the colliding nuclei. The full (open) circles represent the protons (neutrons) from projectile (red) and target (blue) nuclei. The participant nucleons are shown in purple. In panel (a), the arrows indicate the eccentricity vectors (ϵ_n is shown as example) and corresponding reaction (Ψ_{RP}), projectile/target spectator ($\Psi_{SP}^{P,T}$), and participant (multiple Ψ_n , $n \geq 1$) plane angles. Panel (b) shows the outward deflection, indicated by curved arrows, of the spectators and fragmentation products of the projectile ($\eta > 0$) and target ($\eta < 0$) recoil nuclei, such as protons (p), neutrons (n), and nuclei (deuteron, helium, etc.).

Figure 1 sketches the geometry of a non-central heavy-ion collision, divided into the regions of the participant nucleons (i.e. those encountering strong interactions) and the deflected spectator nucleons of the target (T) and projectile (P) nuclei. The geometrical reaction plane, denoted by its angle Ψ_{RP} in Fig. 1a, is spanned by the impact parameter, pointing in the direction of the x_{RP} axis, and the movement direction of the colliding nuclei, which is indicated by the z axis. The fluctuating shape of the energy

density distribution of the collision can be characterized by the eccentricities ε_n for $n > 1$

$$\varepsilon_n e^{in\Psi_n} = -\frac{\int r^n e^{in\varphi} \rho(r, \varphi) r dr d\varphi}{\int r^n \rho(r, \varphi) r dr d\varphi}, \quad (1)$$

where $\rho(r, \varphi)$ is the initial energy or entropy density near midrapidity and (r, φ) are the polar coordinates. Eq. (1) for $n = 2$ gives the standard formula for the ellipticity [29, 30]. In the absence of fluctuations, the azimuthal symmetry plane of the collision is given by the reaction plane. In the presence of fluctuations, the collision symmetry is not described by a single reaction plane, but by multiple participant planes with angles Ψ_n and spectator planes with angles Ψ_{SP}^T and Ψ_{SP}^P . The spectator planes are spanned by the beam direction and the deflection of the spectators, which is determined by the sum of the momenta of the spectator nucleons and fragments. For small fluctuations of the spectator deflection, the target and projectile spectator planes share a common symmetry plane with angle Ψ_{SP} . The sketch is oriented along the reaction plane x_{RP} (i.e. $\Psi_{RP} = 0$), while in the experiment the orientation of the collision relative to the laboratory frame fluctuates from one collision to another. This causes the reaction plane angle to be different from zero.

Figure 1b illustrates a longitudinal view of the early time of a heavy-ion collision, in particular the deflection of the spectators. The fragmentation of the nuclear recoil is a complex process [31] involving the release of protons, neutrons, and other nuclei, which causes a decorrelation of the reaction plane and spectator planes. Additionally, a plane defined only by a subset of the spectator fragments (e.g. only neutrons or protons) can be different from the overall spectator plane orientation illustrated in Fig. 1a. This difference depends on the collision centrality due to the balance between the energy carried by free nucleons and nuclear fragments.

The deflection of the spectators along the spectator planes at LHC collision energies, as illustrated by the red and blue arrows in Fig. 1a, was shown to be outward from the nuclear overlap region, based on the measured directed flow relative to the neutron spectator plane and hydrodynamic model calculations [32]. From measurements of the neutron deflection at the LHC, the transverse momentum exchange between the participants and the spectators has been estimated to be in the order of $20 \text{ MeV}/c$ per nucleon in midcentral collisions [33]. This is about an order of magnitude smaller than the width of the transverse momentum distribution of emitted spectators, which is proportional [34, 35] to the Fermi momentum of $265 \text{ MeV}/c$ [36] for lead nuclei.

Due to the geometry of the collision, the direction in which the spectators are deflected is believed to be strongly correlated to the reaction plane. In collisions with large impact parameters, the smaller number of sources of particle production (number of participants) results in a stronger decorrelation of the participant symmetry plane and the reaction plane. Measurements of the directed flow using the deflection of spectator neutrons showed a small but non-zero decorrelation between the direction of the neutron deflection and the reaction plane orientation, in addition to a relative decorrelation of the neutron spectator planes originating from the projectile and target nuclei, respectively [33]. A strong correlation between the participant and spectator planes is expected in midcentral collisions because of the dominance of the elliptic flow [37]. Together with measurements relative to the participant planes, a measurement relative to the spectator deflection provides unique information about spatial orientation of the participant zone relative to the geometrical orientation of the colliding nuclei [33].

Hydrodynamic model calculations with small viscosities indicate an approximately linear response to the initial eccentricities for elliptic and triangular flow [38]. In ideal hydrodynamics, the elliptic flow v_2 is proportional to the initial eccentricity [39]

$$v_2 \propto \kappa_2 \varepsilon_2. \quad (2)$$

This has been demonstrated by the comparison of measurements relative to the participant plane with eccentricities from different initial state model calculations [25]. The scaling coefficient κ_2 is related to

the initial entropy density. In ideal hydrodynamics, it is estimated from the final state multiplicity dN_{ch}/dy per unit of the overlap area S [40–42]

$$\frac{v_2}{\varepsilon_2} \propto \frac{1}{S} \frac{dN_{\text{ch}}}{dy}. \quad (3)$$

Following Ref. [25], the area S is defined as $S = 4\pi\sigma_x\sigma_y$, where σ_x is the spatial width of the participant zone along the reaction plane direction (x_{RP}) and σ_y is along the transverse direction (y). This scaling can be tested by comparing different collision systems and their dependence on centrality or center-of-mass energy. Such a scaling is broken by viscous effects, which depend on the magnitude of the temperature-dependent specific shear and bulk viscosities [41]. Even for an ideal fluid, the scaling can be broken during the final stages of the evolution before freeze-out [41].

One of the largest uncertainties in the description of heavy-ion collisions is the pattern of fluctuations in the initial state that results in large uncertainties of the extracted QGP transport properties [43, 44]. Among the observables that quantify the effects of initial state fluctuations are the cumulants [29], which can be used to decompose both the spatial and momentum anisotropies. The cumulants of the eccentricity distribution describe the shape of the initial state fluctuations. There are different models describing this initial state and its fluctuations. One of the simplest analytical descriptions is the Bessel-Gaussian model (BGM) [45] in which many sources of entropy production result in a two-dimensional Gaussian shape of fluctuations, where all higher-order ($m \geq 4$) eccentricity cumulants, $\varepsilon_2\{m\}$, are degenerate and equal to the reaction plane eccentricity

$$\varepsilon_2\{2\} > \varepsilon_2\{4\} = \varepsilon_{\text{RP}}. \quad (4)$$

The BGM is only applicable to small fluctuations. The elliptic-power model (EPM) is a more general analytical model, which is also applicable for the description of large fluctuations [11]. In the EPM, the degeneracy of higher-order cumulants is broken and therefore

$$\varepsilon_2\{2\} > \varepsilon_2\{4\} > \varepsilon_{\text{RP}}. \quad (5)$$

There are a number of Monte Carlo models of the initial state that either implement a specific physical mechanism of pre-equilibrium entropy production, for example IP-Glasma [46], or do not assume a specific mechanism, such as TRENTo [12]. In TRENTo, the entropy production in the participant zone is parameterized by the transverse density of the participating nucleons, i.e. the participant thickness. Each of these models is characterized by specific signatures of the eccentricity cumulants and their relationships. The importance of subnucleonic degrees of freedom for modeling fluctuations in central collisions has been highlighted in Ref. [47].

One can probe the initial state eccentricities by comparing the ratios of eccentricity cumulants defined by Eq. (1) to equivalent flow observables, if the fluid response is linear as given by Eq. (2). These observables can be constructed through angular correlations of the emitted particles and the symmetry planes

$$v_2\{\Psi_{\text{SP}}\} = \langle\langle \cos 2(\varphi_1 - \Psi_{\text{SP}}) \rangle\rangle, \quad (6)$$

$$v_2\{2, |\Delta\eta|\} = \sqrt{\langle\langle \cos 2(\varphi_1 - \varphi_2) \rangle\rangle} = \langle v_2^2 \rangle^{\frac{1}{2}}, \quad (7)$$

$$v_2\{4\} = [2\langle\langle \cos 2(\varphi_1 - \varphi_2) \rangle\rangle^2 - \langle\langle \cos 2(\varphi_1 - \varphi_2 + \varphi_3 - \varphi_4) \rangle\rangle]^{\frac{1}{4}} = [2\langle v_2^2 \rangle^2 - \langle v_2^4 \rangle]^{\frac{1}{4}}. \quad (8)$$

Here φ_i ($i = 1 \dots 4$) are the azimuthal angles of the produced particles, $\langle \dots \rangle$ is the average over all collisions, and $\langle\langle \dots \rangle\rangle$ is the average over all particles in a given transverse momentum window in all collisions. The $v_2\{\Psi_{\text{SP}}\}$ is the elliptic flow measured relative to the spectator plane with angle Ψ_{SP} , where fluctuations of the spectator symmetry planes are assumed to be small. The $v_2\{2\}$ and $v_2\{4\}$ are estimators of elliptic flow coefficients whose equations, including p_{T} -dependence, are derived from the two- and four-particle cumulants [48, 49]. The variable $|\Delta\eta|$ in Eq. (7) refers to the minimum pseudorapidity (η) separation between the two correlated particles. The observables $v_2\{\Psi_{\text{SP}}\}$, $v_2\{4\}$, and $v_2\{2, |\Delta\eta|\}$ may deviate from $v_2\{\Psi_{\text{RP}}\}$, which is the unmeasurable momentum anisotropy relative to the

reaction plane. The comparison of ratios of the measured anisotropic flow coefficients to their respective eccentricities is instrumental for identifying the most realistic model of the initial state.

The transverse momentum dependence of the flow coefficients v_n allows one to study if there is a common origin of anisotropy at different transverse momentum scales due to initial state eccentricity fluctuations. The main source of anisotropy for soft ($p_T < 3 \text{ GeV}/c$) particle production is the collective expansion of the QGP [38]. At significantly larger p_T , the dominant contribution to v_n is the path length dependent energy loss of the jet propagating through the azimuthally asymmetric medium oriented along Ψ_n [50]. A significant transverse momentum dependence of flow fluctuations relative to the participant planes is observed [50] in central collisions and within large experimental uncertainties in midcentral collisions. Given that the spectators only probe the early time evolution of the collision and provide sensitivity to a different symmetry plane, the transverse momentum dependence of the ratio $v_2\{\Psi_{\text{SP}}\}/v_2\{4\}$ can be used as an additional observable to investigate the origin of flow fluctuations.

An accurate determination of the flow coefficients relative to the spectator plane, in particular of the elliptic flow $v_2\{\Psi_{\text{SP}}\}$, is also crucial for the search of the chiral magnetic effect (CME) [51, 52]. Because the magnetic field orientation is correlated more strongly to the spectator deflection than to the participant plane orientation, the measurement relative to both planes allows the separation of the CME signal from the background correlations coupled to the elliptic flow [52–57].

In this letter, the charged particle elliptic flow relative to the neutron spectator deflection, $v_2\{\Psi_{\text{SP}}\}$, and to the participant plane, quantified by $v_2\{2, |\Delta\eta| > 1\}$ and $v_2\{4\}$, is reported as a function of centrality and transverse momentum for collisions of Pb ions at a center-of-mass energy per nucleon–nucleon pair of $\sqrt{s_{\text{NN}}} = 2.76 \text{ TeV}$ and Xe ions at $\sqrt{s_{\text{NN}}} = 5.44 \text{ TeV}$. The comparison with different initial state models, such as BGM, EPM, and TRENTo, and the scaling properties of v_2/ϵ_2 are also presented.

ALICE is a dedicated heavy-ion experiment at the LHC. A detailed description of the detector and its performance can be found elsewhere [58, 59]. The trajectories of the charged particles are reconstructed using the Inner Tracking System (ITS) and the Time Projection Chamber (TPC) [60, 61]. The neutron spectator deflection is estimated using the neutron Zero Degree Calorimeters (ZDC) [62]. The ZDC consist of two detectors with a 2×2 transverse segmentation. During the Pb–Pb (Xe–Xe) data-taking, the ZDC were placed 114 m (112.5 m) away from the collision point on both sides of the experiment, named A and C side, covering the pseudorapidity interval $|\eta| > 8.78$ (8.77). The collision centrality is reconstructed using the energy deposition in the forward V0 scintillator arrays [63].

About 10 (1) million of minimum bias [59] Pb–Pb (Xe–Xe) collisions collected in the year 2010 (2017) are analyzed. This corresponds to collisions in the 5–70% centrality range and a reconstructed primary collision vertex located within $\pm 10 \text{ cm}$ along the beam direction from the nominal interaction point. Outside of this centrality range, the deflection of the spectators cannot be reliably reconstructed because of the small number of detected neutron spectators in central collisions and the large fraction of spectator neutrons that are not detected by the ZDC in peripheral collisions because they are bound in charged fragments and thus deflected by the LHC magnets.

The charged particles are selected within the range of pseudorapidity $|\eta| < 0.8$ and transverse momentum $p_T > 0.2 \text{ GeV}/c$. The tracks are reconstructed using the combined information from the ITS and the TPC detectors. A minimum of 70 TPC space points (out of a maximum of 159) and a minimum of two ITS hits, with at least one in one of the two innermost layers, are required for all tracks. A reduced χ^2 per TPC space point (ITS hit) in the range 0.1–4 (less than 36) is required. Only tracks with a distance of closest approach to the primary vertex position smaller than 3.2 cm in the beam direction and within a radius of 2.4 cm in the transverse plane are considered.

The observables in Eqs. (6) to (8), are calculated using flow vectors q_n^K of harmonic n in each collision as

$$q_n^K = x_n^K + iy_n^K = \sum_{j \in K} (w_j)^p e^{in\varphi_j} \Bigg/ \sum_{j \in K} (w_j)^p, \quad (9)$$

where K denotes either the reconstructed tracks $K = T$ or the two ZDC subdetectors $K = A, C$.

For the second harmonic flow vector of the reconstructed tracks q_2^T , the w_j and φ_j are the weight and azimuthal angle of the j -th track, respectively. The weights in the q_2^T calculation are defined by the inverse product $w = 1/(\epsilon dN/d\varphi)$ of the p_T -dependent reconstruction efficiency ϵ and the measured non-uniform azimuthal angle distribution $dN/d\varphi$ of the charged particles. The $dN/d\varphi$ is calculated as a function of the pseudorapidity of the particles and the primary vertex position along the beam direction. The impact of the correction for the non-uniform azimuthal acceptance of the tracks is negligible. The reconstruction efficiency correction is derived from a Monte Carlo simulation using the HIJING [64] heavy-ion event generator to simulate collisions and GEANT3 [65] to model particle transport through the ALICE detector material. It is applied to all measurements of the p_T -integrated flow coefficients. The power p in Eq. (9) corresponds to the correction of the non-uniform azimuthal acceptance and reconstruction efficiency in the multi-particle cumulant method [66]. It only differs from unity for q_2^T . The $v_2\{2, |\Delta\eta| > 1\}$ and $v_2\{4\}$ are calculated from flow vectors defined in Eq. (9) using the multi-particle cumulant approach [66]. In the measurement of $v_2\{2, |\Delta\eta| > 1\}$, a pseudorapidity separation of $|\Delta\eta| > 1$ is applied as it largely suppresses few-particle correlations (so called non-flow), such as those originating from jets or resonance decays [67].

For the first harmonic flow vectors of the ZDC, q_1^A and q_1^C , φ_j corresponds to the angle of the center of the j -th calorimeter segment and w_j to its measured energy deposition. The indices A and C stand for the subdetectors located on either side of the interaction point. The neutron spectator deflection is estimated with these flow vectors. The beam configuration can result in an average shift of the spectator neutron distributions in the transverse plane of the ZDC that are corrected by a data-driven procedure (re-centering)

$$q'_n = q_n - \langle q_n \rangle. \quad (10)$$

To account for changing beam conditions, the re-centering correction is calculated as a function of the centrality, and the three dimensional position of the collision vertex for each data-taking period. The elliptic flow $v_2\{\Psi_{\text{SP}}\}$ is calculated from an average of three independent estimates using the scalar product method with mixed harmonics [68]

$$v_2\{\Psi_{\text{SP}}\} = \frac{2}{3} \left(\frac{\langle x_2^T x_1^A x_1^C \rangle}{\langle x_1^A x_1^C \rangle} - \frac{\langle x_2^T y_1^A y_1^C \rangle}{\langle y_1^A y_1^C \rangle} + \sqrt{\frac{\langle y_2^T x_1^A y_1^C \rangle \langle y_2^T y_1^A x_1^C \rangle}{\langle x_1^A x_1^C \rangle \langle y_1^A y_1^C \rangle}} \right), \quad (11)$$

which corresponds to a measurement of elliptic flow relative to the common spectator plane Ψ_{SP} . The numerical coefficient (2/3) arises from (1/3) which corresponds to an average of the three independent terms in Eq.(11) and an additional factor two from an expectation that correlators in the numerators of individual terms gives $(1/4)v_2\{\Psi_{\text{SP}}\}R_1^2\{\text{ZDC}\}$ and in the denominators $(1/2)R_1^2\{\text{ZDC}\}$, where $R_1\{\text{ZDC}\}$ is a convolution of the directed flow of spectators with the ZDC response.

The systematic uncertainties are evaluated from variations of the analysis procedure. The total systematic uncertainty is given by the square root of the sum in quadrature of the differences in the results obtained from each significant variation. A variation is considered significant, if $\Delta R/\Delta\sigma > 1$ [69], where ΔR is the difference between results from a given variation and the default analysis procedure. The variable $\Delta\sigma$ is the square root of the difference between the corresponding squared statistical uncertainties.

The description of systematic uncertainties related to measurements of $v_2\{2, |\Delta\eta| > 1\}$ and $v_2\{4\}$ is presented in Ref. [70]. The details of the systematic uncertainty evaluation for $v_2\{\Psi_{\text{SP}}\}$ are described

below. The largest source of systematic uncertainty is due to spurious correlations which are not corrected by the recentering procedure. These affect the denominators in Eq. (11), which are determined by the diagonal correlations $\langle x_1^A x_1^C \rangle$ and $\langle y_1^A y_1^C \rangle$. The corresponding relative uncertainty, labeled as ZDC scale uncertainty, is evaluated from the off-diagonal correlations $\langle x_1^A y_1^C \rangle$ and $\langle y_1^A x_1^C \rangle$, which should not contain physical signal, divided by the diagonal correlations. This uncertainty is found to be about 4% (9%) in Pb–Pb (Xe–Xe) collisions for all centrality classes and it is assigned as a fully correlated uncertainty for $v_2\{\Psi_{SP}\}$ results. The observed negative sign of the diagonal correlations indicates a deflection of the neutron spectators in, on average, opposite directions [33]. The off-diagonal correlations may be non-zero because of the specific beam conditions during the LHC operations that may affect the distribution of neutrons impinging ZDC, such as the beam divergence at the interaction point.

The second largest contribution to the relative uncertainty comes from the differences among the three independent estimates of $v_2\{\Psi_{SP}\}$ corresponding to the three terms in Eq. (11) and amounts to lower than 2%. The uncertainty due to the implementation of the flow vector re-centering procedure, defined by Eq. (10), is evaluated by comparing to results from an iterative procedure. In the latter, each of the four iterations consists of one coarse-binned four-dimensional re-centering step followed by four fine-grained one-dimensional steps as a function of the centrality and the three dimensional position of the collision vertex. The corresponding relative variation is below 1%. Introducing an additional equalization of the average ZDC signals in the flow vector calculation in Eq. (9) amounts to a relative uncertainty less than 1%.

The systematic uncertainties related to the reconstruction of charged particle tracks and to the secondary particle contamination are evaluated by varying the track selection criteria. A relative uncertainty from changing the selection of the distance to the primary vertex of the collision as a function of particle p_T , the minimum number of TPC clusters and the reduced χ^2 per TPC cluster is about 1.5%. No significant difference between results for positively and negatively charged particles is observed. A relative uncertainty of 0.7% on the p_T -dependent track reconstruction efficiency was estimated from the difference between the results obtained with an efficiency calculation using all primary tracks and those using only tracks of primary π , K, p, μ , and e. The uncertainty due to the non-uniform acceptance correction, estimated from the difference of results with and without applying the $1/(dN/d\varphi)$ weights in Eq. (9), is not significant. An uncertainty due to the centrality determination reaching up to 2% in the most peripheral collisions is estimated from the difference of the results obtained when using an alternative centrality estimator based on the multiplicity of hits in the ITS. The effects of the TPC misalignment and the beam optics at the interaction point are estimated to be smaller than 0.5% by comparing results obtained with different magnetic field polarities of the ALICE solenoid. The impact on the results of the variation of charged particle acceptance in pseudorapidity within the fiducial volume of ALICE is probed by reducing the accepted range of the position of the reconstructed primary vertex of the collisions along the beam direction from the nominal ± 10 cm to ± 8 cm. It yields no significant change of $v_2\{\Psi_{SP}\}$. For the ratios $v_2\{2, |\Delta\eta| > 1\} / v_2\{4\}$ and $v_2\{\Psi_{SP}\} / v_2\{4\}$ most of the common sources of systematic uncertainties cancel out. In addition, the bin-to-bin uncorrelated uncertainties cancel in the p_T -dependence of these ratios.

The results for the elliptic flow coefficients relative to the spectator symmetry plane, $v_2\{\Psi_{SP}\}$, and the participant plane, $v_2\{2\}$ and $v_2\{4\}$, as a function of the centrality in Pb–Pb and Xe–Xe collisions are shown in the upper panels of Fig. 2. In both Pb–Pb and Xe–Xe collisions, the maximum of $v_2\{\Psi_{SP}\}$ is located in the 35–45% centrality range with a hint of being shifted towards more peripheral collisions for smaller systems. The difference between $v_2\{2, |\Delta\eta| > 1\}$ and $v_2\{4\}$ is due to fluctuations in the participant zone, which have been extensively studied [8, 71–73]. In peripheral collisions, this difference may also originate from residual few-particle correlations. In midcentral collisions, $v_2\{\Psi_{SP}\}$ and $v_2\{4\}$ are similar as expected from the BGM (see Eq. (4)).

To study the differences between the flow observables in detail, the lower panels of Fig. 2 show the

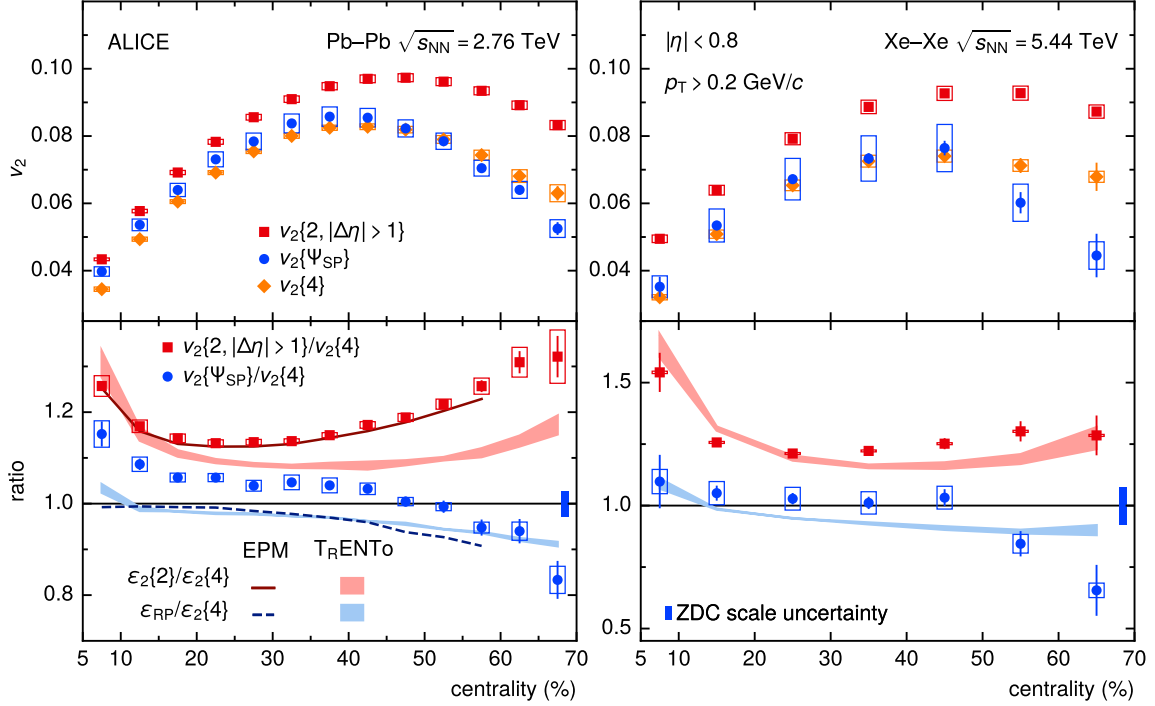


Figure 2: (color online) (upper panels) Elliptic flow relative to the spectator plane, $v_2\{\Psi_{SP}\}$, and to the participant plane, $v_2\{2, |\Delta\eta| > 1\}$ and $v_2\{4\}$, as a function of centrality in Pb–Pb (left) and Xe–Xe (right) collisions. (bottom panels) Ratios of the elliptic flow $v_2\{\Psi_{SP}\}$ and $v_2\{2, |\Delta\eta| > 1\}$ to $v_2\{4\}$. The dashed (solid) lines show the eccentricity ratios of ϵ_{RP} ($\epsilon_2\{2\}$) to $\epsilon_2\{4\}$ from the elliptic power model. The corresponding eccentricity ratios for T_RENTo are shown as solid bands. The error bars (open boxes) indicate statistical (systematic) uncertainties. The bin-to-bin uncorrelated uncertainties and the correlated ones are combined for $v_2\{\Psi_{SP}\}$ results. For the ratio $v_2\{\Psi_{SP}\}/v_2\{4\}$, the ZDC scale uncertainties are shown separately as solid boxes centered at unity on the right side of the lower panels.

centrality dependence of the ratios of $v_2\{2, |\Delta\eta| > 1\}$ and $v_2\{\Psi_{SP}\}$ to $v_2\{4\}$ as well as the ratios of the respective eccentricity cumulants calculated from the EPM and the T_RENTo models. The width of the bands, which represent the T_RENTo calculations, in Fig. 2 indicate the differences between two configurations that are tuned to different experimental data. The model in Ref. [43] uses Pb–Pb collisions at $\sqrt{s_{NN}} = 2.76$ TeV and $\sqrt{s_{NN}} = 5.02$ TeV, whereas Ref. [44] uses data of Au–Au collisions at $\sqrt{s_{NN}} = 0.2$ TeV and Pb–Pb collisions at $\sqrt{s_{NN}} = 2.76$ TeV. The deformed Woods-Saxon parametrization of Xe nuclei is adopted from Ref. [74]. The considered model calculations do not take into account the subnucleonic degrees of freedom. It was demonstrated in Ref. [25] based on two-particle cumulant measurements that at the LHC they only impact very central (0–5%) Pb–Pb collisions, which is outside of the reported centrality range. The EPM model parameters, which relies on significant differences between higher order cumulants, are only accessible with the larger data sample of Pb–Pb collisions at $\sqrt{s_{NN}} = 5.02$ TeV [70].

In both central and peripheral Pb–Pb collisions, the ratio $v_2\{\Psi_{SP}\}/v_2\{4\}$ strongly deviates from unity, which is the value expected from the BGM for the eccentricity ratio. In midcentral collisions, the measured ratio is smaller than in central collisions, but it is significantly larger than the BGM (unity), EPM and T_RENTo model calculations. The later indicates that the spectator plane becomes decorrelated from the reaction plane and simultaneously more correlated with the participant plane. Thus $v_2\{\Psi_{SP}\}$ becomes closer to $v_2\{2, |\Delta\eta| > 1\}$, which makes the ratio $v_2\{\Psi_{SP}\}/v_2\{4\}$ above unity. Similar trends are observed in Xe–Xe collisions, however due to the limited size of the data sample the deviations from unity are not significant within the uncertainties except in the most peripheral collisions. A decorrelation

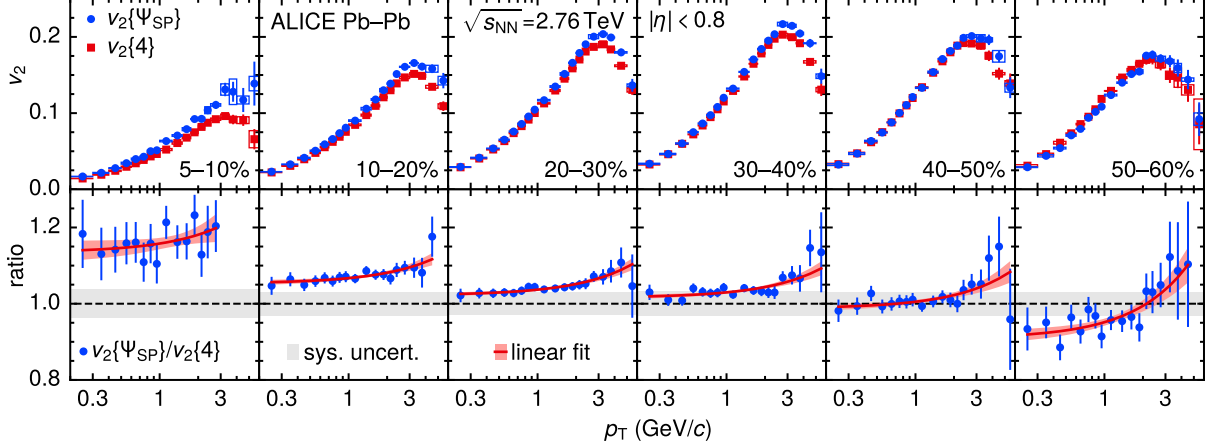


Figure 3: (color online) (upper panels) Elliptic flow relative to the spectator plane, $v_2\{\Psi_{SP}\}$, and to the participant plane, $v_2\{4\}$, as a function of transverse momentum in different centrality classes for Pb–Pb collisions. The linear fits to the ratio $v_2\{\Psi_{SP}\}/v_2\{4\}$ are shown as red lines for the individual centrality classes. The error bars (open boxes) indicate statistical (systematic) uncertainties. The correlated uncertainties, related to the ZDC, and bin-to-bin uncorrelated ones are combined for $v_2\{\Psi_{SP}\}$ (upper panels). For the ratio $v_2\{\Psi_{SP}\}/v_2\{4\}$ (lower panels), the correlated uncertainty is shown by the grey band at unity.

in peripheral collisions is expected due to the small number of sources of particle production (number of participants), as well as due to the decreasing fraction of energy carried by the neutrons measured with the ZDC relative to the unmeasured energy of protons and other charged nuclear fragments.

In central collisions, despite the largest number of particle-producing sources, the fluctuations are also large and deviations of the $v_2\{\Psi_{SP}\}/v_2\{4\}$ ratio from unity are growing, which is in contrast to BGM expectations. The deviation from unity is also large compared to the EPM calculations, which yield a value close to unity in central collisions. This can be either due to (a) a small number of spectators emitted in these collisions which increases the spectator plane fluctuations (decorrelation) around the reaction plane and consequently increases the magnitude of $v_2\{\Psi_{SP}\}$, (b) the strengthening of the correlation between Ψ_{SP} and Ψ_2 angles, or (c) specific geometry fluctuations and/or correlated local particle production in individual participating nucleon–nucleon interactions that reduce $v_2\{4\}$. In midcentral and peripheral collisions, both models predict a small deviation from unity for $\epsilon_{RP}/\epsilon_2\{4\}$, which is expected for small fluctuations given by the second equality of Eq. (4) and due to the small skewness observed in Ref. [70]. The ratio of $\epsilon_2\{2\}/\epsilon_2\{4\}$ from the TRENTo model shows smaller fluctuations compared to the tuned-on-data EPM calculations and the measured $v_2\{2, |\Delta\eta| > 1\}/v_2\{4\}$.

The upper panels of Fig. 3 show the dependence of the elliptic flow coefficients $v_2\{\Psi_{SP}\}$ and $v_2\{4\}$ on transverse momentum for different centrality classes in Pb–Pb collisions. The lower panels of Fig. 3 show the ratio $v_2\{\Psi_{SP}\}/v_2\{4\}$ as a function of p_T for different centrality classes. To quantify the possible dependence of $v_2\{\Psi_{SP}\}/v_2\{4\}$ on p_T , the ratio was fitted with a linear function in the range 0.2–6 GeV/c. The slopes of the linear fit in different centrality classes are: 2.31 ± 2.17 (5–10%), 1.41 ± 0.48 (10–20%), 1.48 ± 0.36 (20–30%), 1.40 ± 0.42 (30–40%), 1.74 ± 0.65 (40–50%), 4.29 ± 1.34 (50–60%) in units of $100/(\text{GeV}/c)$. There are indications for a non-flat transverse momentum dependence of $v_2\{\Psi_{SP}\}/v_2\{4\}$ with a statistical significance of about $2.5\text{--}4\sigma$ in all centrality classes except for 5–10% central collisions where it is only 1σ . These observations are important for understanding to which extent the momentum anisotropy at low and intermediate transverse momentum has a common origin from the fluctuating initial state anisotropy in the coordinate space and quantifying the effects of momentum-dependent flow magnitude and angle decorrelation [22, 75].

The scaling behavior of the elliptic flow with the initial state eccentricities, as suggested by Eq. (3), is

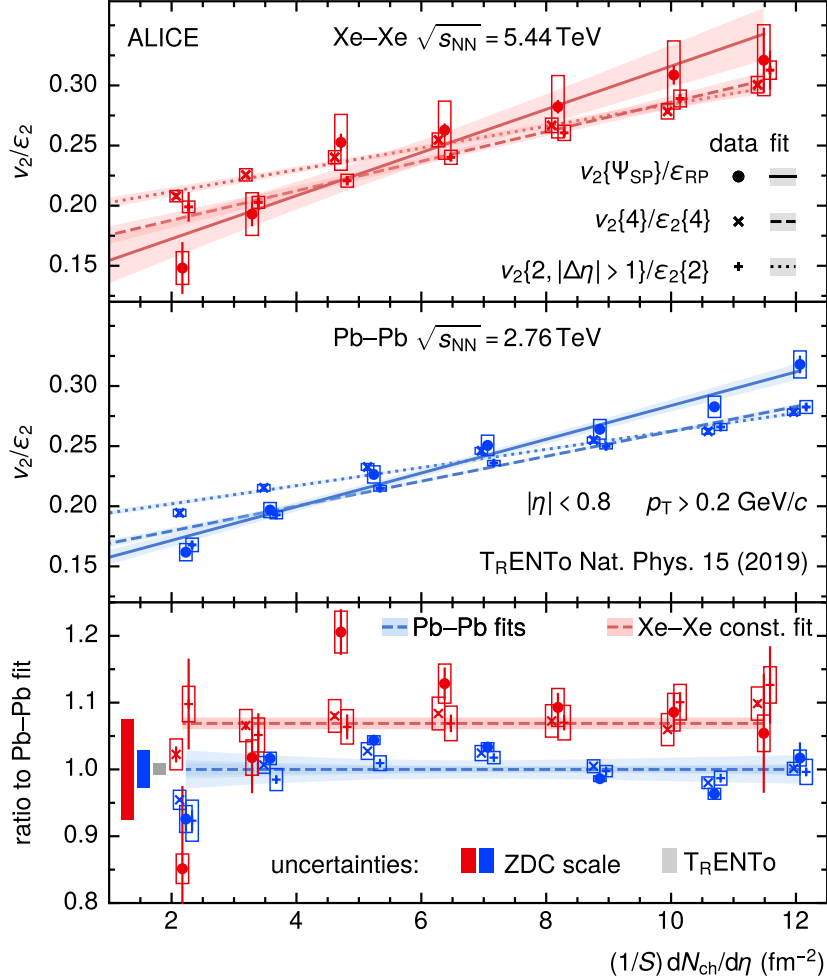


Figure 4: (color online) Ratios of v_2/ε_2 as a function of $(1/S)dN_{\text{ch}}/d\eta$ in Xe–Xe (top panel) and Pb–Pb (middle panel) collisions. The Linear fit functions to v_2/ε_2 in the top and middle panels are shown by lines. The bands show the uncertainty of the fit. (bottom panel) The ratio of v_2/ε_2 to the linear Pb–Pb fits shown in the middle panel. The data points of $v_2\{2, |\Delta\eta| > 1\}$, $v_2\{4\}$ are shifted by -0.1 and $+0.1$ along $(1/S)dN_{\text{ch}}/d\eta$ for better visibility. The error bars (open boxes) indicate statistical (systematic) uncertainties. The ZDC scale uncertainty, due to residual correlations in the determination of the denominators in Eq. (11), and the bin-to-bin uncorrelated one are combined for $v_2\{\Psi_{\text{SP}}\}$ (top and middle panels). For the ratio of $v_2\{\Psi_{\text{SP}}\}$ to the Pb–Pb fit (bottom panel), the ZDC scale uncertainty is separated and is shown by the solid boxes on the left side of the bottom panel. The grey box at unity in the bottom panel on the left side shows the variation depending on the T_RENTo configuration. The blue horizontal band (bottom panel) represents the relative uncertainties of the individual linear fits to the Pb–Pb data from the middle panel. The red horizontal line (bottom panel) shows a combined fit of a constant function to the Xe–Xe data and its uncertainty.

shown in Fig. 4. The top and middle panels present the ratio v_2/ε_2 as a function of the charged particle multiplicity density per unit of the nuclei overlap area $(1/S)dN_{\text{ch}}/d\eta$ for the elliptic flow coefficients $v_2\{2, |\Delta\eta| > 1\}$, $v_2\{4\}$, and $v_2\{\Psi_{\text{SP}}\}$. The area S and the corresponding eccentricities are calculated from the T_RENTo model using the configuration from Ref. [43]. The experimental data points for $dN_{\text{ch}}/d\eta$ as a function of centrality are taken from Ref. [76] for Pb–Pb and from Ref. [74] for Xe–Xe collisions. The lines represent linear fits to the ratios $v_2\{\Psi_{\text{SP}}\}/\varepsilon_{\text{RP}}$, $v_2\{2, |\Delta\eta| > 1\}/\varepsilon_2\{2\}$, and $v_2\{4\}/\varepsilon_2\{4\}$.

Deviations from the scaling behavior are quantified in the bottom panel of Fig. 4, which shows v_2/ε_2 divided by the respective linear fits of the Pb–Pb measurement. The small differences between eccentricities

calculated from the two T_RENTo configurations are reflected in the height of the solid gray box on the left side. The splitting between the individual observables for a given collision system may be sensitive to the chosen association of eccentricities to flow coefficients. A relative deviation of $(7.0 \pm 0.9)\%$ from the scaling given by Eq. (3) between the two collision systems is extracted from a constant line fit to the Xe–Xe data and by propagating uncertainties of the Pb–Pb data. An additional variation of $+1.8\%$ is estimated from the difference between the two T_RENTo configurations. It is similar for the different flow coefficients and only weakly depends on the multiplicity density or collision centrality. This collision system dependence may be sensitive to the details of the initial state models [25, 77] and to viscous effects in the expansion of the QGP [41]. Together with the results on the centrality and transverse momentum dependence, shown in Figs. 2 and 3, the scaling presented in Fig. 4 provides new experimental constraints to both the initial conditions and the transport coefficients of the QGP produced in heavy-ion collisions.

In summary, the elliptic flow of charged particles at midrapidity ($|\eta| < 0.8$) relative to the neutron spectator plane $v_2 \{\Psi_{SP}\}$ is measured in Pb–Pb at $\sqrt{s_{NN}} = 2.76$ TeV and Xe–Xe at $\sqrt{s_{NN}} = 5.44$ TeV collisions as a function of the centrality and as a function of the transverse momentum in different centrality classes. The measurements are compared to results of elliptic flow relative to the participant plane obtained from two and four-particle correlations. Both in central and peripheral collisions, the ratio $v_2 \{\Psi_{SP}\} / v_2 \{4\}$ strongly deviates from the respective ratio of the eccentricities, $\varepsilon_{RP}/\varepsilon_2 \{4\}$, predicted by the T_RENTo and EPM models of the initial state fluctuations. The observations can be interpreted as a decorrelation of the neutron spectator plane and the reaction plane due to the fragmentation of the recoil from the colliding nuclei which indicates an incomplete description of initial state fluctuations in the models. A transverse momentum dependence of the ratio $v_2 \{\Psi_{SP}\} / v_2 \{4\}$ is observed with $2.5\text{--}4\sigma$ significance in all but the most central collisions. This is an important experimental input for understanding whether the momentum anisotropies at low and intermediate transverse momentum have a common origin in the initial state fluctuations. The ratios of elliptic flow coefficients to the initial state eccentricities for Xe–Xe and Pb–Pb collisions reveal a relative deviation from the scaling with the initial entropy density of $(7.0 \pm 0.9)\%$ with an additional variation of $+1.8\%$ when including RHIC data in the T_RENTo parameter extraction. The deviation is independent of the charged particle multiplicity density, which provides new experimental constraints for viscous effects in the expansion of the quark–gluon plasma produced in heavy-ion collisions at the LHC.

Acknowledgements

The ALICE Collaboration would like to thank all its engineers and technicians for their invaluable contributions to the construction of the experiment and the CERN accelerator teams for the outstanding performance of the LHC complex. The ALICE Collaboration gratefully acknowledges the resources and support provided by all Grid centres and the Worldwide LHC Computing Grid (WLCG) collaboration. The ALICE Collaboration acknowledges the following funding agencies for their support in building and running the ALICE detector: A. I. Alikhanyan National Science Laboratory (Yerevan Physics Institute) Foundation (ANSL), State Committee of Science and World Federation of Scientists (WFS), Armenia; Austrian Academy of Sciences, Austrian Science Fund (FWF): [M 2467-N36] and Nationalstiftung für Forschung, Technologie und Entwicklung, Austria; Ministry of Communications and High Technologies, National Nuclear Research Center, Azerbaijan; Conselho Nacional de Desenvolvimento Científico e Tecnológico (CNPq), Financiadora de Estudos e Projetos (Finep), Fundação de Amparo à Pesquisa do Estado de São Paulo (FAPESP) and Universidade Federal do Rio Grande do Sul (UFRGS), Brazil; Bulgarian Ministry of Education and Science, within the National Roadmap for Research Infrastructures 2020-2027 (object CERN), Bulgaria; Ministry of Education of China (MOEC) , Ministry of Science & Technology of China (MSTC) and National Natural Science Foundation of China (NSFC), China; Ministry of Science and Education and Croatian Science Foundation, Croatia; Centro de Aplicaciones Tecnológicas y Desarrollo Nuclear (CEADEN), Cubaenergía, Cuba; Ministry of Education, Youth and Sports of the

Czech Republic, Czech Republic; The Danish Council for Independent Research | Natural Sciences, the VILLUM FONDEN and Danish National Research Foundation (DNRF), Denmark; Helsinki Institute of Physics (HIP), Finland; Commissariat à l’Energie Atomique (CEA) and Institut National de Physique Nucléaire et de Physique des Particules (IN2P3) and Centre National de la Recherche Scientifique (CNRS), France; Bundesministerium für Bildung und Forschung (BMBF) and GSI Helmholtzzentrum für Schwerionenforschung GmbH, Germany; General Secretariat for Research and Technology, Ministry of Education, Research and Religions, Greece; National Research, Development and Innovation Office, Hungary; Department of Atomic Energy Government of India (DAE), Department of Science and Technology, Government of India (DST), University Grants Commission, Government of India (UGC) and Council of Scientific and Industrial Research (CSIR), India; National Research and Innovation Agency - BRIN, Indonesia; Istituto Nazionale di Fisica Nucleare (INFN), Italy; Japanese Ministry of Education, Culture, Sports, Science and Technology (MEXT) and Japan Society for the Promotion of Science (JSPS) KAKENHI, Japan; Consejo Nacional de Ciencia (CONACYT) y Tecnología, through Fondo de Cooperación Internacional en Ciencia y Tecnología (FONCICYT) and Dirección General de Asuntos del Personal Académico (DGAPA), Mexico; Nederlandse Organisatie voor Wetenschappelijk Onderzoek (NWO), Netherlands; The Research Council of Norway, Norway; Commission on Science and Technology for Sustainable Development in the South (COMSATS), Pakistan; Pontificia Universidad Católica del Perú, Peru; Ministry of Education and Science, National Science Centre and WUT ID-UB, Poland; Korea Institute of Science and Technology Information and National Research Foundation of Korea (NRF), Republic of Korea; Ministry of Education and Scientific Research, Institute of Atomic Physics, Ministry of Research and Innovation and Institute of Atomic Physics and University Politehnica of Bucharest, Romania; Ministry of Education, Science, Research and Sport of the Slovak Republic, Slovakia; National Research Foundation of South Africa, South Africa; Swedish Research Council (VR) and Knut & Alice Wallenberg Foundation (KAW), Sweden; European Organization for Nuclear Research, Switzerland; Suranaree University of Technology (SUT), National Science and Technology Development Agency (NSTDA), Thailand Science Research and Innovation (TSRI) and National Science, Research and Innovation Fund (NSRF), Thailand; Turkish Energy, Nuclear and Mineral Research Agency (TENMAK), Turkey; National Academy of Sciences of Ukraine, Ukraine; Science and Technology Facilities Council (STFC), United Kingdom; National Science Foundation of the United States of America (NSF) and United States Department of Energy, Office of Nuclear Physics (DOE NP), United States of America. In addition, individual groups or members have received support from: Marie Skłodowska Curie, Strong 2020 - Horizon 2020, European Research Council (grant nos. 824093, 896850, 950692), European Union; Academy of Finland (Center of Excellence in Quark Matter) (grant nos. 346327, 346328), Finland; Programa de Apoyos para la Superación del Personal Académico, UNAM, Mexico.

References

- [1] S. Ryu, J. F. Paquet, C. Shen, G. S. Denicol, B. Schenke, S. Jeon, and C. Gale, “Importance of the bulk viscosity of QCD in ultrarelativistic heavy-ion collisions”, *Phys. Rev. Lett.* **115** (2015) 132301, arXiv:1502.01675 [nucl-th].
- [2] B. Schenke, S. Jeon, and C. Gale, “Elliptic and triangular flow in event-by-event (3+1)D viscous hydrodynamics”, *Phys. Rev. Lett.* **106** (2011) 042301, arXiv:1009.3244 [hep-ph].
- [3] M. Miller and R. Snellings, “Eccentricity fluctuations and its possible effect on elliptic flow measurements”, arXiv:nucl-ex/0312008.
- [4] **PHOBOS** Collaboration, B. Alver *et al.*, “The eccentricities of flow: Elliptic flow fluctuations and evidence for transverse localization in the initial state of the matter in relativistic heavy ion collisions”, in *International Workshop on Hadron Physics and Property of High Baryon Density Matter*. 2, 2007. arXiv:nucl-ex/0702029.

- [5] **STAR** Collaboration, P. Sorensen, “Elliptic flow fluctuations in Au + Au collisions at $\sqrt{s_{NN}} = 200$ GeV”, *J. Phys. G* **35** (2008) 104102, arXiv:0808.0356 [nucl-ex].
- [6] B. Alver and G. Roland, “Collision geometry fluctuations and triangular flow in heavy-ion collisions”, *Phys. Rev. C* **81** (2010) 054905, arXiv:1003.0194 [nucl-th]. [Erratum: Phys.Rev.C 82, 039903 (2010)].
- [7] **PHENIX** Collaboration, A. Adare *et al.*, “Measurements of higher-order flow harmonics in Au+Au collisions at $\sqrt{s_{NN}} = 200$ GeV”, *Phys. Rev. Lett.* **107** (2011) 252301, arXiv:1105.3928 [nucl-ex].
- [8] **ALICE** Collaboration, K. Aamodt *et al.*, “Higher harmonic anisotropic flow measurements of charged particles in Pb–Pb collisions at $\sqrt{s_{NN}} = 2.76$ TeV”, *Phys. Rev. Lett.* **107** (2011) 032301, arXiv:1105.3865 [nucl-ex].
- [9] **STAR** Collaboration, L. Adamczyk *et al.*, “Third harmonic flow of charged particles in Au+Au collisions at $\sqrt{s_{NN}} = 200$ GeV”, *Phys. Rev. C* **88** (2013) 014904, arXiv:1301.2187 [nucl-ex].
- [10] **STAR** Collaboration, L. Adamczyk *et al.*, “Beam energy dependence of the third harmonic of azimuthal correlations in Au+Au collisions at RHIC”, *Phys. Rev. Lett.* **116** (2016) 112302, arXiv:1601.01999 [nucl-ex].
- [11] L. Yan, J.-Y. Ollitrault, and A. M. Poskanzer, “Eccentricity distributions in nucleus-nucleus collisions”, *Phys. Rev. C* **90** (2014) 024903, arXiv:1405.6595 [nucl-th].
- [12] J. S. Moreland, J. E. Bernhard, and S. A. Bass, “Alternative ansatz to wounded nucleon and binary collision scaling in high-energy nuclear collisions”, *Phys. Rev. C* **92** (2015) 011901, arXiv:1412.4708 [nucl-th].
- [13] **ALICE** Collaboration, S. Acharya *et al.*, “Characterizing the initial conditions of heavy-ion collisions at the LHC with mean transverse momentum and anisotropic flow correlations”, *Phys. Lett. B* **834** (2022) 137393, arXiv:2111.06106 [nucl-ex].
- [14] **ATLAS** Collaboration, G. Aad *et al.*, “Measurement of the azimuthal anisotropy for charged particle production in $\sqrt{s_{NN}} = 2.76$ TeV lead-lead collisions with the ATLAS detector”, *Phys. Rev. C* **86** (2012) 014907, arXiv:1203.3087 [hep-ex].
- [15] **CMS** Collaboration, S. Chatrchyan *et al.*, “Measurement of higher-order harmonic azimuthal anisotropy in PbPb collisions at $\sqrt{s_{NN}} = 2.76$ TeV”, *Phys. Rev. C* **89** (2014) 044906, arXiv:1310.8651 [nucl-ex].
- [16] **ATLAS** Collaboration, G. Aad *et al.*, “Measurement of the distributions of event-by-event flow harmonics in lead-lead collisions at $\sqrt{s_{NN}} = 2.76$ TeV with the ATLAS detector at the LHC”, *JHEP* **11** (2013) 183, arXiv:1305.2942 [hep-ex].
- [17] **ATLAS** Collaboration, G. Aad *et al.*, “Measurement of event-plane correlations in $\sqrt{s_{NN}} = 2.76$ TeV lead-lead collisions with the ATLAS detector”, *Phys. Rev. C* **90** (2014) 024905, arXiv:1403.0489 [hep-ex].
- [18] **ATLAS** Collaboration, G. Aad *et al.*, “Measurement of the correlation between flow harmonics of different order in lead-lead collisions at $\sqrt{s_{NN}} = 2.76$ TeV with the ATLAS detector”, *Phys. Rev. C* **92** (2015) 034903, arXiv:1504.01289 [hep-ex].
- [19] **ALICE** Collaboration, J. Adam *et al.*, “Correlated event-by-event fluctuations of flow harmonics in Pb–Pb collisions at $\sqrt{s_{NN}} = 2.76$ TeV”, *Phys. Rev. Lett.* **117** (2016) 182301, arXiv:1604.07663 [nucl-ex].

- [20] ALICE Collaboration, J. Adam *et al.*, “Anisotropic flow of charged particles in Pb–Pb collisions at $\sqrt{s_{\text{NN}}} = 5.02 \text{ TeV}$ ”, *Phys. Rev. Lett.* **116** (2016) 132302, arXiv:1602.01119 [nucl-ex].
- [21] CMS Collaboration, A. M. Sirunyan *et al.*, “Non-gaussian elliptic-flow fluctuations in PbPb collisions at $\sqrt{s_{\text{NN}}} = 5.02 \text{ TeV}$ ”, *Phys. Lett. B* **789** (2019) 643–665, arXiv:1711.05594 [nucl-ex].
- [22] ALICE Collaboration, S. Acharya *et al.*, “Searches for transverse momentum dependent flow vector fluctuations in Pb–Pb and p–Pb collisions at the LHC”, *JHEP* **09** (2017) 032, arXiv:1707.05690 [nucl-ex].
- [23] ALICE Collaboration, S. Acharya *et al.*, “Linear and non-linear flow modes in Pb–Pb collisions at $\sqrt{s_{\text{NN}}} = 2.76 \text{ TeV}$ ”, *Phys. Lett. B* **773** (2017) 68–80, arXiv:1705.04377 [nucl-ex].
- [24] ALICE Collaboration, S. Acharya *et al.*, “Energy dependence and fluctuations of anisotropic flow in Pb–Pb collisions at $\sqrt{s_{\text{NN}}} = 5.02$ and 2.76 TeV ”, *JHEP* **07** (2018) 103, arXiv:1804.02944 [nucl-ex].
- [25] ALICE Collaboration, S. Acharya *et al.*, “Anisotropic flow in Xe–Xe collisions at $\sqrt{s_{\text{NN}}} = 5.44 \text{ TeV}$ ”, *Phys. Lett. B* **784** (2018) 82–95, arXiv:1805.01832 [nucl-ex].
- [26] ALICE Collaboration, S. Acharya *et al.*, “Non-linear flow modes of identified particles in Pb–Pb collisions at $\sqrt{s_{\text{NN}}} = 5.02 \text{ TeV}$ ”, *JHEP* **06** (2020) 147, arXiv:1912.00740 [nucl-ex].
- [27] ALICE Collaboration, S. Acharya *et al.*, “Higher harmonic non-linear flow modes of charged hadrons in Pb–Pb collisions at $\sqrt{s_{\text{NN}}} = 5.02 \text{ TeV}$ ”, *JHEP* **05** (2020) 085, arXiv:2002.00633 [nucl-ex].
- [28] ALICE Collaboration, S. Acharya *et al.*, “Measurements of mixed harmonic cumulants in Pb–Pb collisions at $\sqrt{s_{\text{NN}}} = 5.02 \text{ TeV}$ ”, *Phys. Lett. B* **818** (2021) 136354, arXiv:2102.12180 [nucl-ex].
- [29] D. Teaney and L. Yan, “Triangularity and dipole asymmetry in heavy ion collisions”, *Phys. Rev. C* **83** (2011) 064904, arXiv:1010.1876 [nucl-th].
- [30] L. Yan, “A flow paradigm in heavy-ion collisions”, *Chin. Phys. C* **42** (2018) 042001, arXiv:1712.04580 [nucl-th].
- [31] A. Schüttauf *et al.*, “Universality of spectator fragmentation at relativistic bombarding energies”, *Nucl. Phys. A* **607** (1996) 457–486, arXiv:nucl-ex/9606001.
- [32] S. A. Voloshin and T. Niida, “Ultrarelativistic nuclear collisions: Direction of spectator flow”, *Phys. Rev. C* **94** (2016) 021901, arXiv:1604.04597 [nucl-th].
- [33] ALICE Collaboration, B. Abelev *et al.*, “Directed flow of charged particles at midrapidity relative to the spectator plane in Pb–Pb collisions at $\sqrt{s_{\text{NN}}} = 2.76 \text{ TeV}$ ”, *Phys. Rev. Lett.* **111** (2013) 232302, arXiv:1306.4145 [nucl-ex].
- [34] A. S. Goldhaber, “Statistical models of fragmentation processes”, *Phys. Lett. B* **53** (1974) 306–308.
- [35] D. J. Morrissey, “Systematics of momentum distributions from reactions with relativistic ions”, *Phys. Rev. C* **39** (1989) 460–470.
- [36] E. J. Moniz, I. Sick, R. R. Whitney, J. R. Ficenec, R. D. Kephart, and W. P. Trower, “Nuclear fermi momenta from quasielastic electron scattering”, *Phys. Rev. Lett.* **26** (1971) 445–448.

- [37] **ALICE** Collaboration, K. Aamodt *et al.*, “Harmonic decomposition of two-particle angular correlations in Pb–Pb collisions at $\sqrt{s_{\text{NN}}} = 2.76 \text{ TeV}$ ”, *Phys. Lett. B* **708** (2012) 249–264, arXiv:1109.2501 [nucl-ex].
- [38] Z. Qiu and U. W. Heinz, “Event-by-event shape and flow fluctuations of relativistic heavy-ion collision fireballs”, *Phys. Rev. C* **84** (2011) 024911, arXiv:1104.0650 [nucl-th].
- [39] F. G. Gardim, F. Grassi, M. Luzum, and J.-Y. Ollitrault, “Mapping the hydrodynamic response to the initial geometry in heavy-ion collisions”, *Phys. Rev. C* **85** (2012) 024908, arXiv:1111.6538 [nucl-th].
- [40] S. A. Voloshin and A. M. Poskanzer, “The physics of the centrality dependence of elliptic flow”, *Phys. Lett. B* **474** (2000) 27–32, arXiv:nucl-th/9906075.
- [41] H. Song and U. W. Heinz, “Multiplicity scaling in ideal and viscous hydrodynamics”, *Phys. Rev. C* **78** (2008) 024902, arXiv:0805.1756 [nucl-th].
- [42] U. Heinz and R. Snellings, “Collective flow and viscosity in relativistic heavy-ion collisions”, *Ann. Rev. Nucl. Part. Sci.* **63** (2013) 123–151, arXiv:1301.2826 [nucl-th].
- [43] J. E. Bernhard, J. S. Moreland, and S. A. Bass, “Bayesian estimation of the specific shear and bulk viscosity of quark–gluon plasma”, *Nature Phys.* **15** (2019) 1113–1117.
- [44] **JETSCAPE** Collaboration, D. Everett *et al.*, “Multisystem bayesian constraints on the transport coefficients of QCD matter”, *Phys. Rev. C* **103** (2021) 054904, arXiv:2011.01430 [hep-ph].
- [45] S. A. Voloshin, A. M. Poskanzer, A. Tang, and G. Wang, “Elliptic flow in the gaussian model of eccentricity fluctuations”, *Phys. Lett. B* **659** (2008) 537–541, arXiv:0708.0800 [nucl-th].
- [46] B. Schenke, P. Tribedy, and R. Venugopalan, “Fluctuating glasma initial conditions and flow in heavy ion collisions”, *Phys. Rev. Lett.* **108** (2012) 252301, arXiv:1202.6646 [nucl-th].
- [47] H. Song, S. A. Bass, U. Heinz, T. Hirano, and C. Shen, “200 A GeV Au+Au collisions serve a nearly perfect quark-gluon liquid”, *Phys. Rev. Lett.* **106** (2011) 192301, arXiv:1011.2783 [nucl-th]. [Erratum: Phys.Rev.Lett. 109, 139904 (2012)].
- [48] N. Borghini, P. M. Dinh, and J.-Y. Ollitrault, “A new method for measuring azimuthal distributions in nucleus-nucleus collisions”, *Phys. Rev. C* **63** (2001) 054906, arXiv:nucl-th/0007063.
- [49] A. Bilandzic, R. Snellings, and S. Voloshin, “Flow analysis with cumulants: Direct calculations”, *Phys. Rev. C* **83** (2011) 044913, arXiv:1010.0233 [nucl-ex].
- [50] **ALICE** Collaboration, B. Abelev *et al.*, “Anisotropic flow of charged hadrons, pions and (anti-)protons measured at high transverse momentum in Pb-Pb collisions at $\sqrt{s_{\text{NN}}} = 2.76 \text{ TeV}$ ”, *Phys. Lett. B* **719** (2013) 18–28, arXiv:1205.5761 [nucl-ex].
- [51] **STAR** Collaboration, M. Abdallah *et al.*, “Search for the chiral magnetic effect with isobar collisions at $\sqrt{s_{\text{NN}}} = 200 \text{ GeV}$ by the STAR collaboration at the BNL Relativistic Heavy Ion Collider”, *Phys. Rev. C* **105** (2022) 014901, arXiv:2109.00131 [nucl-ex].
- [52] **STAR** Collaboration, M. Abdallah *et al.*, “Search for the chiral magnetic effect via charge-dependent azimuthal correlations relative to spectator and participant planes in Au+Au collisions at $\sqrt{s_{\text{NN}}} = 200 \text{ GeV}$ ”, *Phys. Rev. Lett.* **128** (2022) 092301, arXiv:2106.09243 [nucl-ex].

- [53] S. A. Voloshin, “Parity violation in hot QCD: How to detect it”, *Phys. Rev. C* **70** (2004) 057901, arXiv:hep-ph/0406311.
- [54] F. Wang, “Effects of cluster particle correlations on local parity violation observables”, *Phys. Rev. C* **81** (2010) 064902, arXiv:0911.1482 [nucl-ex].
- [55] A. Bzdak, V. Koch, and J. Liao, “Remarks on possible local parity violation in heavy ion collisions”, *Phys. Rev. C* **81** (2010) 031901, arXiv:0912.5050 [nucl-th].
- [56] H.-j. Xu, J. Zhao, X. Wang, H. Li, Z.-W. Lin, C. Shen, and F. Wang, “Varying the chiral magnetic effect relative to flow in a single nucleus-nucleus collision”, *Chin. Phys. C* **42** (2018) 084103, arXiv:1710.07265 [nucl-th].
- [57] S. A. Voloshin, “Estimate of the signal from the chiral magnetic effect in heavy-ion collisions from measurements relative to the participant and spectator flow planes”, *Phys. Rev. C* **98** (2018) 054911, arXiv:1805.05300 [nucl-ex].
- [58] ALICE Collaboration, K. Aamodt *et al.*, “The ALICE experiment at the CERN LHC”, *Journal of Instrumentation* **3** (Aug, 2008) S08002–S08002. <https://doi.org/10.1088/1748-0221/3/08/s08002>.
- [59] ALICE Collaboration, B. B. Abelev *et al.*, “Performance of the ALICE experiment at the CERN LHC”, *Int. J. Mod. Phys. A* **29** (2014) 1430044, arXiv:1402.4476 [nucl-ex].
- [60] ALICE Collaboration, G. Dellacasa *et al.*, “ALICE technical design report of the inner tracking system (ITS)”, *CERN-LHCC-99-12* (1999).
- [61] J. Alme *et al.*, “The ALICE TPC, a large 3-dimensional tracking device with fast readout for ultra-high multiplicity events”, *Nucl. Instrum. Meth. A* **622** (2010) 316–367, arXiv:1001.1950 [physics.ins-det].
- [62] ALICE Collaboration, G. Dellacasa *et al.*, “ALICE technical design report of the zero degree calorimeter (ZDC)”, *CERN-LHCC-99-05* (1999).
- [63] ALICE Collaboration, E. Abbas *et al.*, “Performance of the ALICE VZERO system”, *JINST* **8** (2013) P10016, arXiv:1306.3130 [nucl-ex].
- [64] M. Gyulassy and X.-N. Wang, “HIJING 1.0: A monte carlo program for parton and particle production in high-energy hadronic and nuclear collisions”, *Comput. Phys. Commun.* **83** (1994) 307, arXiv:nucl-th/9502021.
- [65] R. Brun, F. Bruyant, M. Maire, A. C. McPherson, and P. Zanarini, *GEANT 3: user’s guide Geant 3.10, Geant 3.11; rev. version*. CERN, Geneva, 1987. <https://cds.cern.ch/record/1119728>.
- [66] A. Bilandzic, C. H. Christensen, K. Gulbrandsen, A. Hansen, and Y. Zhou, “Generic framework for anisotropic flow analyses with multiparticle azimuthal correlations”, *Phys. Rev. C* **89** (2014) 064904, arXiv:1312.3572 [nucl-ex].
- [67] ALICE Collaboration, B. B. Abelev *et al.*, “Multiparticle azimuthal correlations in p–Pb and Pb–Pb collisions at the CERN Large Hadron Collider”, *Phys. Rev. C* **90** (2014) 054901, arXiv:1406.2474 [nucl-ex].
- [68] I. Selyuzhenkov and S. Voloshin, “Effects of non-uniform acceptance in anisotropic flow measurement”, *Phys. Rev. C* **77** (2008) 034904, arXiv:0707.4672 [nucl-th].

- [69] R. Barlow, “Systematic errors: Facts and fictions”, in *Conference on Advanced Statistical Techniques in Particle Physics*, pp. 134–144. 7, 2002. [arXiv:hep-ex/0207026](#).
- [70] **ALICE** Collaboration, S. Acharya *et al.*, “Energy dependence and fluctuations of anisotropic flow in Pb-Pb collisions at $\sqrt{s_{\text{NN}}} = 5.02$ and 2.76 TeV”, *JHEP* **07** (2018) 103, [arXiv:1804.02944](#) [nucl-ex].
- [71] **STAR** Collaboration, G. Agakishiev *et al.*, “Energy and system-size dependence of two- and four-particle v_2 measurements in heavy-ion collisions at RHIC and their implications on flow fluctuations and nonflow”, *Phys. Rev. C* **86** (2012) 014904, [arXiv:1111.5637](#) [nucl-ex].
- [72] **PHOBOS** Collaboration, B. Alver *et al.*, “Non-flow correlations and elliptic flow fluctuations in gold-gold collisions at $\sqrt{s_{\text{NN}}} = 200$ GeV”, *Phys. Rev. C* **81** (2010) 034915, [arXiv:1002.0534](#) [nucl-ex].
- [73] **PHOBOS** Collaboration, B. Alver *et al.*, “Event-by-event fluctuations of azimuthal particle anisotropy in Au+Au collisions at $\sqrt{s_{\text{NN}}} = 200$ GeV”, *Phys. Rev. Lett.* **104** (2010) 142301, [arXiv:nucl-ex/0702036](#).
- [74] **ALICE** Collaboration, S. Acharya *et al.*, “Centrality and pseudorapidity dependence of the charged-particle multiplicity density in Xe–Xe collisions at $\sqrt{s_{\text{NN}}} = 5.44$ TeV”, *Phys. Lett. B* **790** (2019) 35–48, [arXiv:1805.04432](#) [nucl-ex].
- [75] **CMS** Collaboration, V. Khachatryan *et al.*, “Evidence for transverse momentum and pseudorapidity dependent event plane fluctuations in PbPb and pPb collisions”, *Phys. Rev. C* **92** (2015) 034911, [arXiv:1503.01692](#) [nucl-ex].
- [76] **ALICE** Collaboration, K. Aamodt *et al.*, “Centrality dependence of the charged-particle multiplicity density at mid-rapidity in Pb–Pb collisions at $\sqrt{s_{\text{NN}}} = 2.76$ TeV”, *Phys. Rev. Lett.* **106** (2011) 032301, [arXiv:1012.1657](#) [nucl-ex].
- [77] **STAR** Collaboration, S. A. Voloshin, “Energy and system size dependence of charged particle elliptic flow and v_2/ε scaling”, *J. Phys. G* **34** (2007) S883–886, [arXiv:nucl-ex/0701038](#).

A The ALICE Collaboration

- S. Acharya ^{123,131}, D. Adamová ⁸⁵, A. Adler⁶⁹, G. Aglieri Rinella ³², M. Agnello ²⁹, N. Agrawal ⁵⁰, Z. Ahammed ¹³¹, S. Ahmad ¹⁵, S.U. Ahn ⁷⁰, I. Ahuja ³⁷, A. Akindinov ¹³⁹, M. Al-Turany ⁹⁷, D. Aleksandrov ¹³⁹, B. Alessandro ⁵⁵, H.M. Alfanda ⁶, R. Alfaro Molina ⁶⁶, B. Ali ¹⁵, Y. Ali ¹³, A. Alici ²⁵, N. Alizadehvandchali ¹¹², A. Alkin ³², J. Alme ²⁰, G. Alocco ⁵¹, T. Alt ⁶³, I. Altsybev ¹³⁹, M.N. Anaam ⁶, C. Andrei ⁴⁵, A. Andronic ¹³⁴, V. Anguelov ⁹⁴, F. Antinori ⁵³, P. Antonioli ⁵⁰, C. Anuj ¹⁵, N. Apadula ⁷³, L. Aphectche ¹⁰², H. Appelshäuser ⁶³, S. Arcelli ²⁵, R. Arnaldi ⁵⁵, I.C. Arsene ¹⁹, M. Arslanbek ¹³⁶, A. Augustinus ³², R. Averbbeck ⁹⁷, S. Aziz ¹²⁷, M.D. Azmi ¹⁵, A. Badalà ⁵², Y.W. Baek ⁴⁰, X. Bai ⁹⁷, R. Bailhache ⁶³, Y. Bailung ⁴⁷, R. Bala ⁹⁰, A. Balbino ²⁹, A. Baldissari ¹²⁶, B. Balis ², D. Banerjee ⁴, Z. Banoo ⁹⁰, R. Barbera ²⁶, L. Barioglio ⁹⁵, M. Barlou ⁷⁷, G.G. Barnaföldi ¹³⁵, L.S. Barnby ⁸⁴, V. Barret ¹²³, L. Barreto ¹⁰⁸, C. Bartels ¹¹⁵, K. Barth ³², E. Bartsch ⁶³, F. Baruffaldi ²⁷, N. Bastid ¹²³, S. Basu ⁷⁴, G. Batigne ¹⁰², D. Battistini ⁹⁵, B. Batyunya ¹⁴⁰, D. Bauri ⁴⁶, J.L. Bazo Alba ¹⁰⁰, I.G. Bearden ⁸², C. Beattie ¹³⁶, P. Becht ⁹⁷, D. Behera ⁴⁷, I. Belikov ¹²⁵, A.D.C. Bell Hecharvarria ¹³⁴, F. Bellini ²⁵, R. Bellwied ¹¹², S. Belokurova ¹³⁹, V. Belyaev ¹³⁹, G. Bencedi ^{135,64}, S. Beole ²⁴, A. Bercuci ⁴⁵, Y. Berdnikov ¹³⁹, A. Berdnikova ⁹⁴, L. Bergmann ⁹⁴, M.G. Besou ⁶², L. Betev ³², P.P. Bhaduri ¹³¹, A. Bhasin ⁹⁰, I.R. Bhat ⁹⁰, M.A. Bhat ⁴, B. Bhattacharjee ⁴¹, L. Bianchi ²⁴, N. Bianchi ⁴⁸, J. Bielčík ³⁵, J. Bielčíková ⁸⁵, J. Biernat ¹⁰⁵, A. Bilandzic ⁹⁵, G. Biro ¹³⁵, S. Biswas ⁴, J.T. Blair ¹⁰⁶, D. Blau ¹³⁹, M.B. Blidaru ⁹⁷, N. Bluhm ³⁸, C. Blume ⁶³, G. Boca ^{21,54}, F. Bock ⁸⁶, T. Bodova ²⁰, A. Bogdanov ¹³⁹, S. Boi ²², J. Bok ⁵⁷, L. Boldziszár ¹³⁵, A. Bolozdynya ¹³⁹, M. Bombara ³⁷, P.M. Bond ³², G. Bonomi ^{130,54}, H. Borel ¹²⁶, A. Borissov ¹³⁹, H. Bossi ¹³⁶, E. Botta ²⁴, L. Bratrud ⁶³, P. Braun-Munzinger ⁹⁷, M. Bregant ¹⁰⁸, M. Broz ³⁵, G.E. Bruno ^{96,31}, M.D. Buckland ¹¹⁵, D. Budnikov ¹³⁹, H. Buesching ⁶³, S. Bufalino ²⁹, O. Bugnon ¹⁰², P. Buhler ¹⁰¹, Z. Buthelezi ^{67,119}, J.B. Butt ¹³, A. Bylinkin ¹¹⁴, S.A. Bysiak ¹⁰⁵, M. Cai ^{27,6}, H. Caines ¹³⁶, A. Caliva ⁹⁷, E. Calvo Villar ¹⁰⁰, J.M.M. Camacho ¹⁰⁷, P. Camerini ²³, F.D.M. Canedo ¹⁰⁸, M. Carabas ¹²², F. Carnesecchi ³², R. Caron ^{124,126}, J. Castillo Castellanos ¹²⁶, F. Catalano ²⁹, C. Ceballos Sanchez ¹⁴⁰, I. Chakaberia ⁷³, P. Chakraborty ⁴⁶, S. Chandra ¹³¹, S. Chapelard ³², M. Chartier ¹¹⁵, S. Chattopadhyay ¹³¹, S. Chattopadhyay ⁹⁸, T.G. Chavez ⁴⁴, T. Cheng ⁶, C. Cheshkov ¹²⁴, B. Cheynis ¹²⁴, V. Chibante Barroso ³², D.D. Chinellato ¹⁰⁹, E.S. Chizzali ^{II,95}, J. Cho ⁵⁷, S. Cho ⁵⁷, P. Chochula ³², P. Christakoglou ⁸³, C.H. Christensen ⁸², P. Christiansen ⁷⁴, T. Chujo ¹²¹, M. Ciacco ²⁹, C. Cicalo ⁵¹, L. Cifarelli ²⁵, F. Cindolo ⁵⁰, M.R. Ciupek ⁹⁷, G. Clai ^{III,50}, F. Colamaria ⁴⁹, J.S. Colburn ⁹⁹, D. Colella ^{96,31}, A. Collu ⁷³, M. Colocci ³², M. Concas ^{IV,55}, G. Conesa Balbastre ⁷², Z. Conesa del Valle ¹²⁷, G. Contin ²³, J.G. Contreras ³⁵, M.L. Coquet ¹²⁶, T.M. Cormier ^{I,86}, P. Cortese ^{129,55}, M.R. Cosentino ¹¹⁰, F. Costa ³², S. Costanza ^{21,54}, P. Crochet ¹²³, R. Cruz-Torres ⁷³, E. Cuautle ⁶⁴, P. Cui ⁶, L. Cunqueiro ⁸⁶, A. Dainese ⁵³, M.C. Danisch ⁹⁴, A. Danu ⁶², P. Das ⁷⁹, P. Das ⁴, S. Das ⁴, S. Dash ⁴⁶, R.M.H. David ⁴⁴, A. De Caro ²⁸, G. de Cataldo ⁴⁹, L. De Cilladi ²⁴, J. de Cuveland ³⁸, A. De Falco ²², D. De Gruttola ²⁸, N. De Marco ⁵⁵, C. De Martin ²³, S. De Pasquale ²⁸, S. Deb ⁴⁷, H.F. Degenhardt ¹⁰⁸, K.R. Deja ¹³², R. Del Grande ⁹⁵, L. Dello Stritto ²⁸, W. Deng ⁶, P. Dhankher ¹⁸, D. Di Bari ³¹, A. Di Mauro ³², R.A. Diaz ^{140,7}, T. Dietel ¹¹¹, Y. Ding ^{124,6}, R. Divià ³², D.U. Dixit ¹⁸, Ø. Djupsland ²⁰, U. Dmitrieva ¹³⁹, A. Dobrin ⁶², B. Dönigus ⁶³, A.K. Dubey ¹³¹, J.M. Dubinski ¹³², A. Dubla ⁹⁷, S. Dudi ⁸⁹, P. Dupieux ¹²³, M. Durkac ¹⁰⁴, N. Dzalaiava ¹², T.M. Eder ¹³⁴, R.J. Ehlers ⁸⁶, V.N. Eikeland ²⁰, F. Eisenhut ⁶³, D. Elia ⁴⁹, B. Erazmus ¹⁰², F. Ercolelli ²⁵, F. Erhardt ⁸⁸, M.R. Ersdal ²⁰, B. Espagnon ¹²⁷, G. Eulisse ³², D. Evans ⁹⁹, S. Evdokimov ¹³⁹, L. Fabbietti ⁹⁵, M. Faggion ²⁷, J. Faivre ⁷², F. Fan ⁶, W. Fan ⁷³, A. Fantoni ⁴⁸, M. Fasel ⁸⁶, P. Fecchio ²⁹, A. Feliciello ⁵⁵, G. Feofilov ¹³⁹, A. Fernández Téllez ⁴⁴, M.B. Ferrer ³², A. Ferrero ¹²⁶, A. Ferretti ²⁴, V.J.G. Feuillard ⁹⁴, J. Figiel ¹⁰⁵, V. Filova ³⁵, D. Finogeev ¹³⁹, F.M. Fionda ⁵¹, G. Fiorenza ⁹⁶, F. Flor ¹¹², A.N. Flores ¹⁰⁶, S. Foertsch ⁶⁷, I. Fokin ⁹⁴, S. Fokin ¹³⁹, E. Fragiocomo ⁵⁶, E. Frajna ¹³⁵, U. Fuchs ³², N. Funicello ²⁸, C. Furget ⁷², A. Furs ¹³⁹, J.J. Gaardhøje ⁸², M. Gagliardi ²⁴, A.M. Gago ¹⁰⁰, A. Gal ¹²⁵, C.D. Galvan ¹⁰⁷, P. Ganoti ⁷⁷, C. Garabatos ⁹⁷, J.R.A. Garcia ⁴⁴, E. Garcia-Solis ⁹, K. Garg ¹⁰², C. Gargiulo ³², A. Garibaldi ⁸⁰, K. Garner ¹³⁴, E.F. Gauger ¹⁰⁶, A. Gautam ¹¹⁴, M.B. Gay Ducati ⁶⁵, M. Germain ¹⁰², S.K. Ghosh ⁴, M. Giacalone ²⁵, P. Gianotti ⁴⁸, P. Giubellino ^{97,55}, P. Giubilato ²⁷, A.M.C. Glaenzer ¹²⁶, P. Glässel ⁹⁴, E. Glimos ¹¹⁸, D.J.Q. Goh ⁷⁵, V. Gonzalez ¹³³, L.H. González-Trueba ⁶⁶, S. Gorbunov ³⁸, M. Gorgon ², L. Görlich ¹⁰⁵, S. Gotovac ³³, V. Grabski ⁶⁶, L.K. Graczykowski ¹³², E. Grecka ⁸⁵, L. Greiner ⁷³, A. Grelli ⁵⁸, C. Grigoras ³², V. Grigoriev ¹³⁹, S. Grigoryan ^{140,1}, F. Grossa ³², J.F. Grosse-Oetringhaus ³², R. Grossi ⁹⁷, D. Grund ³⁵, G.G. Guardiano ¹⁰⁹, R. Guernane ⁷², M. Guilbaud ¹⁰², K. Gulbrandsen ⁸², T. Gunji ¹²⁰, W. Guo ⁶, A. Gupta ⁹⁰, R. Gupta ⁹⁰, S.P. Guzman ⁴⁴, L. Gyulai ¹³⁵, M.K. Habib ⁹⁷, C. Hadjidakis ¹²⁷, H. Hamagaki ⁷⁵, M. Hamid ⁶, Y. Han ¹³⁷, R. Hannigan ¹⁰⁶,

- M.R. Haque ¹³², A. Harlenderova ⁹⁷, J.W. Harris ¹³⁶, A. Harton ⁹, J.A. Hasenbichler ³², H. Hassan ⁸⁶, D. Hatzifotiadou ⁵⁰, P. Hauer ⁴², L.B. Havener ¹³⁶, S.T. Heckel ⁹⁵, E. Hellbär ⁹⁷, H. Helstrup ³⁴, T. Herman ³⁵, G. Herrera Corral ⁸, F. Herrmann ¹³⁴, K.F. Hetland ³⁴, B. Heybeck ⁶³, H. Hillermanns ³², C. Hills ¹¹⁵, B. Hippolyte ¹²⁵, B. Hofman ⁵⁸, B. Hohlweger ⁸³, J. Honermann ¹³⁴, G.H. Hong ¹³⁷, D. Horak ³⁵, A. Horzyk ², R. Hosokawa ¹⁴, Y. Hou ⁶, P. Hristov ³², C. Hughes ¹¹⁸, P. Huhn ⁶³, L.M. Huhta ¹¹³, C.V. Hulse ¹²⁷, T.J. Humanic ⁸⁷, H. Hushnud ⁹⁸, A. Hutson ¹¹², D. Hutter ³⁸, J.P. Iddon ¹¹⁵, R. Ilkaev ¹³⁹, H. Ilyas ¹³, M. Inaba ¹²¹, G.M. Innocenti ³², M. Ippolitov ¹³⁹, A. Isakov ⁸⁵, T. Isidori ¹¹⁴, M.S. Islam ⁹⁸, M. Ivanov ⁹⁷, V. Ivanov ¹³⁹, V. Izucheev ¹³⁹, M. Jablonski ², B. Jacak ⁷³, N. Jacazio ³², P.M. Jacobs ⁷³, S. Jadlovska ¹⁰⁴, J. Jadlovsky ¹⁰⁴, L. Jaffe ³⁸, C. Jahnke ¹⁰⁹, M.A. Janik ¹³², T. Janson ⁶⁹, M. Jercic ⁸⁸, O. Jevons ⁹⁹, A.A.P. Jimenez ⁶⁴, F. Jonas ⁸⁶, P.G. Jones ⁹⁹, J.M. Jowett ^{32,97}, J. Jung ⁶³, M. Jung ⁶³, A. Junique ³², A. Jusko ⁹⁹, M.J. Kabus ^{32,132}, J. Kaewjai ¹⁰³, P. Kalinak ⁵⁹, A.S. Kalteyer ⁹⁷, A. Kalweit ³², V. Kaplin ¹³⁹, A. Karasu Uysal ⁷¹, D. Karatovic ⁸⁸, O. Karavichev ¹³⁹, T. Karavicheva ¹³⁹, P. Karczmarczyk ¹³², E. Karpechev ¹³⁹, V. Kashyap ⁷⁹, A. Kazantsev ¹³⁹, U. Kebschull ⁶⁹, R. Keidel ¹³⁸, D.L.D. Keijdener ⁵⁸, M. Keil ³², B. Ketzer ⁴², A.M. Khan ⁶, S. Khan ¹⁵, A. Khanzadeev ¹³⁹, Y. Kharlov ¹³⁹, A. Khatun ¹⁵, A. Khuntia ¹⁰⁵, B. Kileng ³⁴, B. Kim ¹⁶, C. Kim ¹⁶, D.J. Kim ¹¹³, E.J. Kim ⁶⁸, J. Kim ¹³⁷, J.S. Kim ⁴⁰, J. Kim ⁹⁴, J. Kim ⁶⁸, M. Kim ⁹⁴, S. Kim ¹⁷, T. Kim ¹³⁷, S. Kirsch ⁶³, I. Kisel ³⁸, S. Kiselev ¹³⁹, A. Kisiel ¹³², J.P. Kitowski ², J.L. Klay ⁵, J. Klein ³², S. Klein ⁷³, C. Klein-Bösing ¹³⁴, M. Kleiner ⁶³, T. Klemenz ⁹⁵, A. Kluge ³², A.G. Knospe ¹¹², C. Kobdaj ¹⁰³, T. Kollegger ⁹⁷, A. Kondratyev ¹⁴⁰, N. Kondratyeva ¹³⁹, E. Kondratyuk ¹³⁹, J. Konig ⁶³, S.A. Konigstorfer ⁹⁵, P.J. Konopka ³², G. Kornakov ¹³², S.D. Koryciak ², A. Kotliarov ⁸⁵, O. Kovalenko ⁷⁸, V. Kovalenko ¹³⁹, M. Kowalski ¹⁰⁵, I. Králik ⁵⁹, A. Kravčáková ³⁷, L. Kreis ⁹⁷, M. Krivda ^{99,59}, F. Krizek ⁸⁵, K. Krizkova Gajdosova ³⁵, M. Kroesen ⁹⁴, M. Krüger ⁶³, D.M. Krupova ³⁵, E. Kryshen ¹³⁹, M. Krzewicki ³⁸, V. Kučera ³², C. Kuhn ¹²⁵, P.G. Kuijer ⁸³, T. Kumaoka ¹²¹, D. Kumar ¹³¹, L. Kumar ⁸⁹, N. Kumar ⁸⁹, S. Kundu ³², P. Kurashvili ⁷⁸, A. Kurepin ¹³⁹, A.B. Kurepin ¹³⁹, S. Kushpil ⁸⁵, J. Kvapil ⁹⁹, M.J. Kweon ⁵⁷, J.Y. Kwon ⁵⁷, Y. Kwon ¹³⁷, S.L. La Pointe ³⁸, P. La Rocca ²⁶, Y.S. Lai ⁷³, A. Lakrathok ¹⁰³, M. Lamanna ³², R. Langoy ¹¹⁷, P. Larionov ⁴⁸, E. Laudi ³², L. Lautner ^{32,95}, R. Lavicka ¹⁰¹, T. Lazareva ¹³⁹, R. Lea ^{130,54}, J. Lehrbach ³⁸, R.C. Lemmon ⁸⁴, I. León Monzón ¹⁰⁷, M.M. Lesch ⁹⁵, E.D. Lesser ¹⁸, M. Lettrich ⁹⁵, P. Lévai ¹³⁵, X. Li ¹⁰, X.L. Li ⁶, J. Lien ¹¹⁷, R. Lietava ⁹⁹, B. Lim ¹⁶, S.H. Lim ¹⁶, V. Lindenstruth ³⁸, A. Lindner ⁴⁵, C. Lippmann ⁹⁷, A. Liu ¹⁸, D.H. Liu ⁶, J. Liu ¹¹⁵, I.M. Lofnes ²⁰, V. Loginov ¹³⁹, C. Loizides ⁸⁶, P. Loncar ³³, J.A. Lopez ⁹⁴, X. Lopez ¹²³, E. López Torres ⁷, P. Lu ^{97,116}, J.R. Luhder ¹³⁴, M. Lunardon ²⁷, G. Luparello ⁵⁶, Y.G. Ma ³⁹, A. Maevskaya ¹³⁹, M. Mager ³², T. Mahmoud ⁴², A. Maire ¹²⁵, M. Malaeve ¹³⁹, N.M. Malik ⁹⁰, Q.W. Malik ¹⁹, S.K. Malik ⁹⁰, L. Malinina ^{VII,140}, D. Mal'Kevich ¹³⁹, D. Mallick ⁷⁹, N. Mallick ⁴⁷, G. Mandaglio ^{30,52}, V. Manko ¹³⁹, F. Manso ¹²³, V. Manzari ⁴⁹, Y. Mao ⁶, G.V. Margagliotti ²³, A. Margotti ⁵⁰, A. Marín ⁹⁷, C. Markert ¹⁰⁶, M. Marquard ⁶³, N.A. Martin ⁹⁴, P. Martinengo ³², J.L. Martinez ¹¹², M.I. Martínez ⁴⁴, G. Martínez García ¹⁰², S. Masciocchi ⁹⁷, M. Masera ²⁴, A. Masoni ⁵¹, L. Massacrier ¹²⁷, A. Mastroserio ^{128,49}, A.M. Mathis ⁹⁵, O. Matonoha ⁷⁴, P.F.T. Matuoka ¹⁰⁸, A. Matyja ¹⁰⁵, C. Mayer ¹⁰⁵, A.L. Mazuecos ³², F. Mazzaschi ²⁴, M. Mazzilli ³², J.E. Mdhluli ¹¹⁹, A.F. Mechler ⁶³, Y. Melikyan ¹³⁹, A. Menchaca-Rocha ⁶⁶, E. Meninno ^{101,28}, A.S. Menon ¹¹², M. Meres ¹², S. Mhlanga ^{111,67}, Y. Miake ¹²¹, L. Micheletti ⁵⁵, L.C. Migliorin ¹²⁴, D.L. Mihaylov ⁹⁵, K. Mihaylov ^{140,139}, A.N. Mishra ¹³⁵, D. Miśkowiec ⁹⁷, A. Modak ⁴, A.P. Mohanty ⁵⁸, B. Mohanty ⁷⁹, M. Mohisin Khan ^{V,15}, M.A. Molander ⁴³, Z. Moravcova ⁸², C. Mordasini ⁹⁵, D.A. Moreira De Godoy ¹³⁴, I. Morozov ¹³⁹, A. Morsch ³², T. Mrnjavac ³², V. Muccifora ⁴⁸, E. Mudnic ³³, S. Muhuri ¹³¹, J.D. Mulligan ⁷³, A. Mulliri ²², M.G. Munhoz ¹⁰⁸, R.H. Munzer ⁶³, H. Murakami ¹²⁰, S. Murray ¹¹¹, L. Musa ³², J. Musinsky ⁵⁹, J.W. Myrcha ¹³², B. Naik ¹¹⁹, R. Nair ⁷⁸, B.K. Nandi ⁴⁶, R. Nania ⁵⁰, E. Nappi ⁴⁹, A.F. Nassirpour ⁷⁴, A. Nath ⁹⁴, C. Nattrass ¹¹⁸, A. Neagu ¹⁹, A. Negru ¹²², L. Nellen ⁶⁴, S.V. Nesbo ³⁴, G. Neskovic ³⁸, D. Nesterov ¹³⁹, B.S. Nielsen ⁸², E.G. Nielsen ⁸², S. Nikolaev ¹³⁹, S. Nikulin ¹³⁹, V. Nikulin ¹³⁹, F. Noferini ⁵⁰, S. Noh ¹¹, P. Nomokonov ¹⁴⁰, J. Norman ¹¹⁵, N. Novitzky ¹²¹, P. Nowakowski ¹³², A. Nyanin ¹³⁹, J. Nystrand ²⁰, M. Ogino ⁷⁵, A. Ohlson ⁷⁴, V.A. Okorokov ¹³⁹, J. Oleniacz ¹³², A.C. Oliveira Da Silva ¹¹⁸, M.H. Oliver ¹³⁶, A. Onnerstad ¹¹³, C. Oppedisano ⁵⁵, A. Ortiz Velasquez ⁶⁴, A. Oskarsson ⁷⁴, J. Otwinowski ¹⁰⁵, M. Oya ⁹², K. Oyama ⁷⁵, Y. Pachmayer ⁹⁴, S. Padhan ⁴⁶, D. Pagano ^{130,54}, G. Paic ⁶⁴, A. Palasciano ⁴⁹, S. Panebianco ¹²⁶, J. Park ⁵⁷, J.E. Parkkila ^{32,113}, S.P. Pathak ¹¹², R.N. Patra ⁹⁰, B. Paul ²², H. Pei ⁶, T. Peitzmann ⁵⁸, X. Peng ⁶, L.G. Pereira ⁶⁵, H. Pereira Da Costa ¹²⁶, D. Peresunko ¹³⁹, G.M. Perez ⁷, S. Perrin ¹²⁶, Y. Pestov ¹³⁹, V. Petráček ³⁵, V. Petrov ¹³⁹, M. Petrovici ⁴⁵, R.P. Pezzi ^{102,65}, S. Piano ⁵⁶, M. Pikna ¹², P. Pillot ¹⁰², O. Pinazza ^{50,32}, L. Pinsky ¹¹², C. Pinto ^{95,26}, S. Pisano ⁴⁸,

M. Płoskoń ⁷³, M. Planinic⁸⁸, F. Pliquet ⁶³, M.G. Poghosyan ⁸⁶, S. Politano ²⁹, N. Poljak ⁸⁸, A. Pop ⁴⁵, S. Porteboeuf-Houssais ¹²³, J. Porter ⁷³, V. Pozdniakov ¹⁴⁰, S.K. Prasad ⁴, S. Prasad ⁴⁷, R. Preghenella ⁵⁰, F. Prino ⁵⁵, C.A. Pruneau ¹³³, I. Pshenichnov ¹³⁹, M. Puccio ³², S. Qiu ⁸³, L. Quaglia ²⁴, R.E. Quishpe¹¹², S. Ragoni ⁹⁹, A. Rakotozafindrabe ¹²⁶, L. Ramello ^{129,55}, F. Rami ¹²⁵, S.A.R. Ramirez ⁴⁴, T.A. Rancien ⁷², R. Raniwala ⁹¹, S. Raniwala ⁹¹, S.S. Räsänen ⁴³, R. Rath ⁴⁷, I. Ravasenga ⁸³, K.F. Read ^{86,118}, A.R. Redelbach ³⁸, K. Redlich ^{VI,78}, A. Rehman ²⁰, P. Reichelt ⁶³, F. Reidt ³², H.A. Reme-Ness ³⁴, Z. Rescakova³⁷, K. Reygers ⁹⁴, A. Riabov ¹³⁹, V. Riabov ¹³⁹, R. Ricci ²⁸, T. Richert ⁷⁴, M. Richter ¹⁹, W. Riegler ³², F. Rigg ²⁶, C. Ristea ⁶², M. Rodríguez Cahuantzi ⁴⁴, K. Røed ¹⁹, R. Rogalev ¹³⁹, E. Rogochaya ¹⁴⁰, T.S. Rogoschinski ⁶³, D. Rohr ³², D. Röhrich ²⁰, P.F. Rojas ⁴⁴, S. Rojas Torres ³⁵, P.S. Rokita ¹³², F. Ronchetti ⁴⁸, A. Rosano ^{30,52}, E.D. Rosas ⁶⁴, A. Rossi ⁵³, A. Roy ⁴⁷, P. Roy ⁹⁸, S. Roy ⁴⁶, N. Rubini ²⁵, D. Ruggiano ¹³², R. Rui ²³, B. Rumyantsev¹⁴⁰, P.G. Russek ², R. Russo ⁸³, A. Rustamov ⁸⁰, E. Ryabinkin ¹³⁹, Y. Ryabov ¹³⁹, A. Rybicki ¹⁰⁵, H. Rytkonen ¹¹³, W. Rzesz ¹³², O.A.M. Saarimaki ⁴³, R. Sadek ¹⁰², S. Sadovsky ¹³⁹, J. Saetre ²⁰, K. Šafařík ³⁵, S.K. Saha ¹³¹, S. Saha ⁷⁹, B. Sahoo ⁴⁶, P. Sahoo⁴⁶, R. Sahoo ⁴⁷, S. Sahoo ⁶⁰, D. Sahu ⁴⁷, P.K. Sahu ⁶⁰, J. Saini ¹³¹, K. Sajdakova³⁷, S. Sakai ¹²¹, M.P. Salvat ⁹⁷, S. Sambyal ⁹⁰, T.B. Saramela¹⁰⁸, D. Sarkar ¹³³, N. Sarkar¹³¹, P. Sarma ⁴¹, V. Sarritzu ²², V.M. Sarti ⁹⁵, M.H.P. Sas ¹³⁶, J. Schambach ⁸⁶, H.S. Scheid ⁶³, C. Schiaua ⁴⁵, R. Schicker ⁹⁴, A. Schmah ⁹⁴, C. Schmidt ⁹⁷, H.R. Schmidt ⁹³, M.O. Schmidt ³², M. Schmidt ⁹³, N.V. Schmidt ^{86,63}, A.R. Schmier ¹¹⁸, R. Schotter ¹²⁵, J. Schukraft ³², K. Schwarz ⁹⁷, K. Schweda ⁹⁷, G. Sciolli ²⁵, E. Scomparin ⁵⁵, J.E. Seger ¹⁴, Y. Sekiguchi¹²⁰, D. Sekihata ¹²⁰, I. Selyuzhenkov ^{97,139}, S. Senyukov ¹²⁵, J.J. Seo ⁵⁷, D. Serebryakov ¹³⁹, L. Šerkšnyté ⁹⁵, A. Sevcenco ⁶², T.J. Shaba ⁶⁷, A. Shabanov¹³⁹, A. Shabetai ¹⁰², R. Shahoyan ³², W. Shaikh ⁹⁸, A. Shangaraev ¹³⁹, A. Sharma ⁸⁹, D. Sharma ⁴⁶, H. Sharma ¹⁰⁵, M. Sharma ⁹⁰, N. Sharma ⁸⁹, S. Sharma ⁹⁰, U. Sharma ⁹⁰, A. Shatat ¹²⁷, O. Sheibani¹¹², K. Shigaki ⁹², M. Shimomura ⁷⁶, S. Shirinkin ¹³⁹, Q. Shou ³⁹, Y. Sibiriak ¹³⁹, S. Siddhanta ⁵¹, T. Siemiarczuk ⁷⁸, T.F. Silva ¹⁰⁸, D. Silvermyr ⁷⁴, T. Simantathammakul¹⁰³, R. Simeonov ³⁶, G. Simonetti³², B. Singh ⁹⁰, B. Singh ⁹⁵, R. Singh ⁷⁹, R. Singh ⁹⁰, R. Singh ⁴⁷, V.K. Singh ¹³¹, V. Singhal ¹³¹, T. Sinha ⁹⁸, B. Sitar ¹², M. Sitta ^{129,55}, T.B. Skaali¹⁹, G. Skorodumovs ⁹⁴, M. Slupecki ⁴³, N. Smirnov ¹³⁶, R.J.M. Snellings ⁵⁸, E.H. Solheim ¹⁹, C. Soncco¹⁰⁰, J. Song ¹¹², A. Songmoolnak ¹⁰³, F. Soramel ²⁷, S.P. Sorensen ¹¹⁸, R. Soto Camacho ⁴⁴, R. Spijkers ⁸³, I. Sputowska ¹⁰⁵, J. Staa ⁷⁴, J. Stachel ⁹⁴, I. Stan ⁶², P.J. Steffanic ¹¹⁸, S.F. Stiefelmaier ⁹⁴, D. Stocco ¹⁰², I. Storehaug ¹⁹, M.M. Storetvedt ³⁴, P. Stratmann ¹³⁴, S. Strazzi ²⁵, C.P. Stylianidis⁸³, A.A.P. Suaide ¹⁰⁸, C. Suire ¹²⁷, M. Sukhanov ¹³⁹, M. Suljic ³², V. Sumberia ⁹⁰, S. Sumowidagdo ⁸¹, S. Swain ⁶⁰, A. Szabo ¹², I. Szarka ¹², U. Tabassam ¹³, S.F. Taghavi ⁹⁵, G. Taillepied ^{97,123}, J. Takahashi ¹⁰⁹, G.J. Tambave ²⁰, S. Tang ^{123,6}, Z. Tang ¹¹⁶, J.D. Tapia Takaki ¹¹⁴, N. Tapus ¹²², L.A. Tarasovicova ¹³⁴, M.G. Tarzila ⁴⁵, A. Tauro ³², A. Telesca ³², L. Terlizzi ²⁴, C. Terrevoli ¹¹², G. Tersimonov³, S. Thakur ¹³¹, D. Thomas ¹⁰⁶, R. Tieulent ¹²⁴, A. Tikhonov ¹³⁹, A.R. Timmins ¹¹², M. Tkacik ¹⁰⁴, T. Tkacik ¹⁰⁴, A. Toia ⁶³, N. Topilskaya ¹³⁹, M. Toppi ⁴⁸, F. Torales-Acosta ¹⁸, T. Tork ¹²⁷, A.G. Torres Ramos ³¹, A. Trifiró ^{30,52}, A.S. Triolo ^{30,52}, S. Tripathy ⁵⁰, T. Tripathy ⁴⁶, S. Trogolo ³², V. Trubnikov ³, W.H. Trzaska ¹¹³, T.P. Trzciński ¹³², R. Turrisi ⁵³, T.S. Tveter ¹⁹, K. Ullaland ²⁰, B. Ulukutlu ⁹⁵, A. Uras ¹²⁴, M. Urioni ^{54,130}, G.L. Usai ²², M. Vala ³⁷, N. Valle ²¹, S. Vallero ⁵⁵, L.V.R. van Doremalen ⁵⁸, M. van Leeuwen ⁸³, C.A. van Veen ⁹⁴, R.J.G. van Weelden ⁸³, P. Vande Vyvre ³², D. Varga ¹³⁵, Z. Varga ¹³⁵, M. Varga-Kofarago ¹³⁵, M. Vasileiou ⁷⁷, A. Vasiliev ¹³⁹, O. Vázquez Doce ⁹⁵, O. Vazquez Rueda ⁷⁴, V. Vechernin ¹³⁹, E. Vercellin ²⁴, S. Vergara Limón ⁴⁴, L. Vermunt ⁵⁸, R. Vértesi ¹³⁵, M. Verweij ⁵⁸, L. Vickovic ³³, Z. Vilakazi ¹¹⁹, O. Villalobos Baillie ⁹⁹, G. Vino ⁴⁹, A. Vinogradov ¹³⁹, T. Virgili ²⁸, V. Vislavicius ⁸², A. Vodopyanov ¹⁴⁰, B. Volkel ³², M.A. Völkl ⁹⁴, K. Voloshin ¹³⁹, S.A. Voloshin ¹³³, G. Volpe ³¹, B. von Haller ³², I. Vorobyev ⁹⁵, N. Vozniuk ¹³⁹, J. Vrláková ³⁷, B. Wagner ²⁰, C. Wang ³⁹, D. Wang ³⁹, M. Weber ¹⁰¹, A. Wegrzynek ³², F.T. Weiglhofer ³⁸, S.C. Wenzel ³², J.P. Wessels ¹³⁴, S.L. Weyhmiller ¹³⁶, J. Wiechula ⁶³, J. Wikne ¹⁹, G. Wilk ⁷⁸, J. Wilkinson ⁹⁷, G.A. Willems ¹³⁴, B. Windelband ⁹⁴, M. Winn ¹²⁶, J.R. Wright ¹⁰⁶, W. Wu ³⁹, Y. Wu ¹¹⁶, R. Xu ⁶, A.K. Yadav ¹³¹, S. Yalcin ⁷¹, Y. Yamaguchi ⁹², K. Yamakawa ⁹², S. Yang ²⁰, S. Yano ⁹², Z. Yin ⁶, I.-K. Yoo ¹⁶, J.H. Yoon ⁵⁷, S. Yuan ²⁰, A. Yuncu ⁹⁴, V. Zaccolo ²³, C. Zampolli ³², H.J.C. Zanolli ⁵⁸, F. Zanone ⁹⁴, N. Zardoshti ^{32,99}, A. Zarochentsev ¹³⁹, P. Závada ⁶¹, N. Zaviyalov ¹³⁹, M. Zhalov ¹³⁹, B. Zhang ⁶, S. Zhang ³⁹, X. Zhang ⁶, Y. Zhang ¹¹⁶, M. Zhao ¹⁰, V. Zherebchevskii ¹³⁹, Y. Zhi ¹⁰, N. Zhigareva ¹³⁹, D. Zhou ⁶, Y. Zhou ⁸², J. Zhu ^{97,6}, Y. Zhu ⁶, G. Zinovjev^{1,3}, N. Zurlo ^{130,54}

Affiliation Notes

¹ Deceased

^{II} Also at: Max-Planck-Institut für Physik, Munich, Germany

^{III} Also at: Italian National Agency for New Technologies, Energy and Sustainable Economic Development (ENEA), Bologna, Italy

^{IV} Also at: Dipartimento DET del Politecnico di Torino, Turin, Italy

^V Also at: Department of Applied Physics, Aligarh Muslim University, Aligarh, India

^{VI} Also at: Institute of Theoretical Physics, University of Wroclaw, Poland

^{VII} Also at: An institution covered by a cooperation agreement with CERN

Collaboration Institutes

¹ A.I. Alikhanyan National Science Laboratory (Yerevan Physics Institute) Foundation, Yerevan, Armenia

² AGH University of Krakow, Cracow, Poland

³ Bogolyubov Institute for Theoretical Physics, National Academy of Sciences of Ukraine, Kiev, Ukraine

⁴ Bose Institute, Department of Physics and Centre for Astroparticle Physics and Space Science (CAPSS), Kolkata, India

⁵ California Polytechnic State University, San Luis Obispo, California, United States

⁶ Central China Normal University, Wuhan, China

⁷ Centro de Aplicaciones Tecnológicas y Desarrollo Nuclear (CEADEN), Havana, Cuba

⁸ Centro de Investigación y de Estudios Avanzados (CINVESTAV), Mexico City and Mérida, Mexico

⁹ Chicago State University, Chicago, Illinois, United States

¹⁰ China Institute of Atomic Energy, Beijing, China

¹¹ Chungbuk National University, Cheongju, Republic of Korea

¹² Comenius University Bratislava, Faculty of Mathematics, Physics and Informatics, Bratislava, Slovak Republic

¹³ COMSATS University Islamabad, Islamabad, Pakistan

¹⁴ Creighton University, Omaha, Nebraska, United States

¹⁵ Department of Physics, Aligarh Muslim University, Aligarh, India

¹⁶ Department of Physics, Pusan National University, Pusan, Republic of Korea

¹⁷ Department of Physics, Sejong University, Seoul, Republic of Korea

¹⁸ Department of Physics, University of California, Berkeley, California, United States

¹⁹ Department of Physics, University of Oslo, Oslo, Norway

²⁰ Department of Physics and Technology, University of Bergen, Bergen, Norway

²¹ Dipartimento di Fisica, Università di Pavia, Pavia, Italy

²² Dipartimento di Fisica dell'Università and Sezione INFN, Cagliari, Italy

²³ Dipartimento di Fisica dell'Università and Sezione INFN, Trieste, Italy

²⁴ Dipartimento di Fisica dell'Università and Sezione INFN, Turin, Italy

²⁵ Dipartimento di Fisica e Astronomia dell'Università and Sezione INFN, Bologna, Italy

²⁶ Dipartimento di Fisica e Astronomia dell'Università and Sezione INFN, Catania, Italy

²⁷ Dipartimento di Fisica e Astronomia dell'Università and Sezione INFN, Padova, Italy

²⁸ Dipartimento di Fisica 'E.R. Caianiello' dell'Università and Gruppo Collegato INFN, Salerno, Italy

²⁹ Dipartimento DISAT del Politecnico and Sezione INFN, Turin, Italy

³⁰ Dipartimento di Scienze MIFT, Università di Messina, Messina, Italy

³¹ Dipartimento Interateneo di Fisica 'M. Merlin' and Sezione INFN, Bari, Italy

³² European Organization for Nuclear Research (CERN), Geneva, Switzerland

³³ Faculty of Electrical Engineering, Mechanical Engineering and Naval Architecture, University of Split, Split, Croatia

³⁴ Faculty of Engineering and Science, Western Norway University of Applied Sciences, Bergen, Norway

³⁵ Faculty of Nuclear Sciences and Physical Engineering, Czech Technical University in Prague, Prague, Czech Republic

³⁶ Faculty of Physics, Sofia University, Sofia, Bulgaria

³⁷ Faculty of Science, P.J. Šafárik University, Košice, Slovak Republic

³⁸ Frankfurt Institute for Advanced Studies, Johann Wolfgang Goethe-Universität Frankfurt, Frankfurt, Germany

³⁹ Fudan University, Shanghai, China

⁴⁰ Gangneung-Wonju National University, Gangneung, Republic of Korea

⁴¹ Gauhati University, Department of Physics, Guwahati, India

- ⁴² Helmholtz-Institut für Strahlen- und Kernphysik, Rheinische Friedrich-Wilhelms-Universität Bonn, Bonn, Germany
⁴³ Helsinki Institute of Physics (HIP), Helsinki, Finland
⁴⁴ High Energy Physics Group, Universidad Autónoma de Puebla, Puebla, Mexico
⁴⁵ Horia Hulubei National Institute of Physics and Nuclear Engineering, Bucharest, Romania
⁴⁶ Indian Institute of Technology Bombay (IIT), Mumbai, India
⁴⁷ Indian Institute of Technology Indore, Indore, India
⁴⁸ INFN, Laboratori Nazionali di Frascati, Frascati, Italy
⁴⁹ INFN, Sezione di Bari, Bari, Italy
⁵⁰ INFN, Sezione di Bologna, Bologna, Italy
⁵¹ INFN, Sezione di Cagliari, Cagliari, Italy
⁵² INFN, Sezione di Catania, Catania, Italy
⁵³ INFN, Sezione di Padova, Padova, Italy
⁵⁴ INFN, Sezione di Pavia, Pavia, Italy
⁵⁵ INFN, Sezione di Torino, Turin, Italy
⁵⁶ INFN, Sezione di Trieste, Trieste, Italy
⁵⁷ Inha University, Incheon, Republic of Korea
⁵⁸ Institute for Gravitational and Subatomic Physics (GRASP), Utrecht University/Nikhef, Utrecht, Netherlands
⁵⁹ Institute of Experimental Physics, Slovak Academy of Sciences, Košice, Slovak Republic
⁶⁰ Institute of Physics, Homi Bhabha National Institute, Bhubaneswar, India
⁶¹ Institute of Physics of the Czech Academy of Sciences, Prague, Czech Republic
⁶² Institute of Space Science (ISS), Bucharest, Romania
⁶³ Institut für Kernphysik, Johann Wolfgang Goethe-Universität Frankfurt, Frankfurt, Germany
⁶⁴ Instituto de Ciencias Nucleares, Universidad Nacional Autónoma de México, Mexico City, Mexico
⁶⁵ Instituto de Física, Universidade Federal do Rio Grande do Sul (UFRGS), Porto Alegre, Brazil
⁶⁶ Instituto de Física, Universidad Nacional Autónoma de México, Mexico City, Mexico
⁶⁷ iThemba LABS, National Research Foundation, Somerset West, South Africa
⁶⁸ Jeonbuk National University, Jeonju, Republic of Korea
⁶⁹ Johann-Wolfgang-Goethe Universität Frankfurt Institut für Informatik, Fachbereich Informatik und Mathematik, Frankfurt, Germany
⁷⁰ Korea Institute of Science and Technology Information, Daejeon, Republic of Korea
⁷¹ KTO Karatay University, Konya, Turkey
⁷² Laboratoire de Physique Subatomique et de Cosmologie, Université Grenoble-Alpes, CNRS-IN2P3, Grenoble, France
⁷³ Lawrence Berkeley National Laboratory, Berkeley, California, United States
⁷⁴ Lund University Department of Physics, Division of Particle Physics, Lund, Sweden
⁷⁵ Nagasaki Institute of Applied Science, Nagasaki, Japan
⁷⁶ Nara Women's University (NWU), Nara, Japan
⁷⁷ National and Kapodistrian University of Athens, School of Science, Department of Physics , Athens, Greece
⁷⁸ National Centre for Nuclear Research, Warsaw, Poland
⁷⁹ National Institute of Science Education and Research, Homi Bhabha National Institute, Jatni, India
⁸⁰ National Nuclear Research Center, Baku, Azerbaijan
⁸¹ National Research and Innovation Agency - BRIN, Jakarta, Indonesia
⁸² Niels Bohr Institute, University of Copenhagen, Copenhagen, Denmark
⁸³ Nikhef, National institute for subatomic physics, Amsterdam, Netherlands
⁸⁴ Nuclear Physics Group, STFC Daresbury Laboratory, Daresbury, United Kingdom
⁸⁵ Nuclear Physics Institute of the Czech Academy of Sciences, Husinec-Řež, Czech Republic
⁸⁶ Oak Ridge National Laboratory, Oak Ridge, Tennessee, United States
⁸⁷ Ohio State University, Columbus, Ohio, United States
⁸⁸ Physics department, Faculty of science, University of Zagreb, Zagreb, Croatia
⁸⁹ Physics Department, Panjab University, Chandigarh, India
⁹⁰ Physics Department, University of Jammu, Jammu, India
⁹¹ Physics Department, University of Rajasthan, Jaipur, India
⁹² Physics Program and International Institute for Sustainability with Knotted Chiral Meta Matter (SKCM2), Hiroshima University, Hiroshima, Japan
⁹³ Physikalisches Institut, Eberhard-Karls-Universität Tübingen, Tübingen, Germany

- ⁹⁴ Physikalisches Institut, Ruprecht-Karls-Universität Heidelberg, Heidelberg, Germany
⁹⁵ Physik Department, Technische Universität München, Munich, Germany
⁹⁶ Politecnico di Bari and Sezione INFN, Bari, Italy
⁹⁷ Research Division and ExtreMe Matter Institute EMMI, GSI Helmholtzzentrum für Schwerionenforschung GmbH, Darmstadt, Germany
⁹⁸ Saha Institute of Nuclear Physics, Homi Bhabha National Institute, Kolkata, India
⁹⁹ School of Physics and Astronomy, University of Birmingham, Birmingham, United Kingdom
¹⁰⁰ Sección Física, Departamento de Ciencias, Pontificia Universidad Católica del Perú, Lima, Peru
¹⁰¹ Stefan Meyer Institut für Subatomare Physik (SMI), Vienna, Austria
¹⁰² SUBATECH, IMT Atlantique, Nantes Université, CNRS-IN2P3, Nantes, France
¹⁰³ Suranaree University of Technology, Nakhon Ratchasima, Thailand
¹⁰⁴ Technical University of Košice, Košice, Slovak Republic
¹⁰⁵ The Henryk Niewodniczanski Institute of Nuclear Physics, Polish Academy of Sciences, Cracow, Poland
¹⁰⁶ The University of Texas at Austin, Austin, Texas, United States
¹⁰⁷ Universidad Autónoma de Sinaloa, Culiacán, Mexico
¹⁰⁸ Universidade de São Paulo (USP), São Paulo, Brazil
¹⁰⁹ Universidade Estadual de Campinas (UNICAMP), Campinas, Brazil
¹¹⁰ Universidade Federal do ABC, Santo André, Brazil
¹¹¹ University of Cape Town, Cape Town, South Africa
¹¹² University of Houston, Houston, Texas, United States
¹¹³ University of Jyväskylä, Jyväskylä, Finland
¹¹⁴ University of Kansas, Lawrence, Kansas, United States
¹¹⁵ University of Liverpool, Liverpool, United Kingdom
¹¹⁶ University of Science and Technology of China, Hefei, China
¹¹⁷ University of South-Eastern Norway, Kongsberg, Norway
¹¹⁸ University of Tennessee, Knoxville, Tennessee, United States
¹¹⁹ University of the Witwatersrand, Johannesburg, South Africa
¹²⁰ University of Tokyo, Tokyo, Japan
¹²¹ University of Tsukuba, Tsukuba, Japan
¹²² University Politehnica of Bucharest, Bucharest, Romania
¹²³ Université Clermont Auvergne, CNRS/IN2P3, LPC, Clermont-Ferrand, France
¹²⁴ Université de Lyon, CNRS/IN2P3, Institut de Physique des 2 Infinis de Lyon, Lyon, France
¹²⁵ Université de Strasbourg, CNRS, IPHC UMR 7178, F-67000 Strasbourg, France, Strasbourg, France
¹²⁶ Université Paris-Saclay, Centre d'Etudes de Saclay (CEA), IRFU, Département de Physique Nucléaire (DPhN), Saclay, France
¹²⁷ Université Paris-Saclay, CNRS/IN2P3, IJCLab, Orsay, France
¹²⁸ Università degli Studi di Foggia, Foggia, Italy
¹²⁹ Università del Piemonte Orientale, Vercelli, Italy
¹³⁰ Università di Brescia, Brescia, Italy
¹³¹ Variable Energy Cyclotron Centre, Homi Bhabha National Institute, Kolkata, India
¹³² Warsaw University of Technology, Warsaw, Poland
¹³³ Wayne State University, Detroit, Michigan, United States
¹³⁴ Westfälische Wilhelms-Universität Münster, Institut für Kernphysik, Münster, Germany
¹³⁵ Wigner Research Centre for Physics, Budapest, Hungary
¹³⁶ Yale University, New Haven, Connecticut, United States
¹³⁷ Yonsei University, Seoul, Republic of Korea
¹³⁸ Zentrum für Technologie und Transfer (ZTT), Worms, Germany
¹³⁹ Affiliated with an institute covered by a cooperation agreement with CERN
¹⁴⁰ Affiliated with an international laboratory covered by a cooperation agreement with CERN.